



The optical trapezoid model: A novel approach to remote sensing of soil moisture applied to Sentinel-2 and Landsat-8 observations



Morteza Sadeghi ^{a,*}, Ebrahim Babaian ^b, Markus Tuller ^b, Scott B. Jones ^a

^a Department of Plants, Soils and Climate, Utah State University, Logan, UT, United States

^b Department of Soil, Water and Environmental Science, University of Arizona, Tucson, AZ, United States

ARTICLE INFO

Article history:

Received 8 December 2016

Received in revised form 17 May 2017

Accepted 25 May 2017

Available online 3 June 2017

Keywords:

Satellite remote sensing

Soil moisture

Surface reflectance

Sentinel-2

Landsat-8

ABSTRACT

The “trapezoid” or “triangle” model constitutes the most popular approach to remote sensing (RS) of surface soil moisture based on coupled thermal (i.e., land surface temperature) and optical RS observations. The model, hereinafter referred to as Thermal-Optical TRAapezoid Model (TOTRAM), is based on interpretation of the pixel distribution within the land surface temperature - vegetation index (*LST-VI*) space. TOTRAM suffers from two inherent limitations. It is not applicable to satellites that do not provide thermal data (e.g., Sentinel-2) and it requires parameterization for each individual observation date. To overcome these restrictions we propose a novel OPTical TRAapezoid Model (OPTRAM), which is based on the linear physical relationship between soil moisture and shortwave infrared transformed reflectance (*STR*) and is parameterized based on the pixel distribution within the *STR-VI* space. The OPTRAM-based surface soil moisture estimates derived from Sentinel-2 and Landsat-8 observations for the Walnut Gulch and Little Washita watersheds were compared with ground truth soil moisture data. Results indicate that the prediction accuracies of OPTRAM and TOTRAM are comparable, with OPTRAM only requiring observations in the optical electromagnetic frequency domain. The volumetric moisture content estimation errors of both models were below $0.04 \text{ cm}^3 \text{ cm}^{-3}$ with local calibration and about $0.04\text{--}0.05 \text{ cm}^3 \text{ cm}^{-3}$ without calibration. We also demonstrate that OPTRAM only requires a single universal parameterization for a given location, which is a significant advancement that opens a new avenue for remote sensing of soil moisture.

© 2017 Elsevier Inc. All rights reserved.

1. Introduction

The Earth's surface, which exhibits extreme spatiotemporal moisture variations, controls fundamental hydrological processes such as runoff, infiltration, and evaporation (Vereecken et al., 2008; Robinson et al., 2008; Ochsner et al., 2013). Remote sensing (RS) provides exceedingly powerful means for large-scale characterization and monitoring of soil moisture close to the land surface (~0–5 cm). Because soil optical reflection (Whiting et al., 2004; Tian and Philpot, 2015; Babaian et al., 2016; Zeng et al., 2016), thermal emission (Pratt and Ellyett, 1979; Verstraeten et al., 2006; Hassan-Esfahani et al., 2015), and microwave backscatter (Njoku and Entekhabi, 1996; Das et al., 2008; Mladenova et al., 2014) are highly correlated with soil moisture content, numerous methods for optical, thermal and microwave RS of soil moisture have been developed as discussed in comprehensive reviews by Wang and Qu (2009), Nichols et al. (2011), and Zhang and Zhou (2016).

Microwave RS techniques have shown greater potential for monitoring global scale soil moisture dynamics because microwaves can penetrate through vegetation canopy and underlying soil, especially at lower frequencies (Tabatabaeenejad et al., 2015). However, microwave satellite observations are not well suited for small-scale applications (e.g., field scale) due to their inherently coarse resolution. Optical and thermal satellite observations are commonly utilized to close the scale gap because of their higher spatial resolutions (i.e. meter scale).

The so-called “trapezoid” or “triangle” model is one of the most widely applied approaches to RS of soil moisture utilizing both optical and thermal data. The model, hereinafter termed Thermal-Optical TRAapezoid Model (TOTRAM), is based on the interpretation of the pixel distribution within the *LST-VI* space, where *LST* is the land surface temperature and *VI* is a RS-based vegetation index. Nemani et al. (1993), Carlson et al. (1994), and Moran et al. (1994) were among the first to apply the *LST-VI* space for estimating surface soil moisture or actual evapotranspiration. If a sufficiently large number of pixels exist and cloud and standing surface water pixels are removed from the pixel distribution, the shape of the pixel envelope resembles a triangle or a trapezoid (Carlson, 2013). The success of TOTRAM can be attributed to the ease of parameterization that mainly relies on optical and thermal RS observations and does not require ancillary atmospheric and surface

* Corresponding author at: 4820 Old Main Hill, Logan, UT 84322-4820, United States.

E-mail addresses: morteza.sadeghi@usu.edu (M. Sadeghi),

ebabaeian@email.arizona.edu (E. Babaian), mtuller@email.arizona.edu (M. Tuller),

scott.jones@usu.edu (S.B. Jones).

data (Carlson, 2007). Over the last two decades, this simple approach has been successfully applied for estimating surface soil moisture (Gillies et al., 1997; Sandholt et al., 2002; Goward et al., 2002; Wan et al., 2004; Mallick et al., 2009; Patel et al., 2009; Han et al., 2010; Wang et al., 2011).

More recently, several modifications to the conventional trapezoid model have been proposed. To improve prediction accuracy of TOTRAM, Rahimzadeh-Bajgiran et al. (2013) introduced nonlinear relationships between soil moisture and *LST* rather than the linear relationship assumed in the original method. Following Stisen et al. (2008), Zhang et al. (2014) replaced *LST* in the trapezoid with mid-morning *LST* rise to minimize errors associated with RS-based *LST* retrieval. Shafian (2014) and Shafian and Maas (2015a, 2015b) further simplified the trapezoid model by replacing *LST* with the raw digital number of the thermal infrared bands. Sun (2016) proposed a two-stage trapezoid considering that the *LST* of a vegetated surface is less responsive to surface soil moisture variations than the *LST* of a bare soil surface. This is because vegetation can access deep soil moisture to sustain transpiration. The *LST*-VI method is discussed in detail in Carlson (2007) and Petropoulos et al. (2009).

Despite its obvious success, the application of TOTRAM suffers from two inherent limitations. The first limitation is that TOTRAM requires concurrent optical and thermal observations. TOTRAM was initially conceptualized for instruments consisting of both optical and thermal sensors. Hence, this limitation is intrinsic to the approach and precludes application of TOTRAM to satellites such as Sentinel-2, a 2015-launched high spatiotemporal resolution satellite with 13 spectral bands in the optical domain, but no thermal band. The second limitation is that TOTRAM requires time consuming and computationally demanding individual parameterization/calibration for each observation date, because the *LST* not only depends on soil moisture but also on ambient atmospheric parameters such as near surface air temperature, relative humidity, and wind speed (Mallick et al., 2009).

Because surface reflectance, unlike *LST*, does not significantly vary with the ambient atmospheric parameters, optical RS can potentially resolve the two limitations of TOTRAM. Several indices that utilize optical observations have been proposed for soil moisture and drought monitoring (Table 1). Most indices are based on triangular or trapezoidal spaces from pixel distributions of optical observations in different electromagnetic frequency bands. For example, the Perpendicular Drought Index, *PDI* (Ghulam et al., 2007a), the Distance Drought Index, *DDI* (Qin et al., 2010), and the Triangle Soil Moisture Index, *TSMI* (Amani et al., 2016) are derived from the $R_{red} - R_{NIR}$ triangular space [R_{red} and R_{NIR} : red and near infrared (NIR) band reflectance, respectively]. The Shortwave-infrared Perpendicular Drought Index, *SPDI* (Ghulam et al., 2007c) and the Modified Shortwave-

infrared Perpendicular Drought Index, *MSPDI* (Feng et al., 2013) are parameterized based on the $R_{SWIR} - R_{NIR}$ and $R_{\Sigma} - R_{\Delta}$ trapezoidal space, respectively [R_{SWIR} : shortwave infrared (SWIR) band reflectance, $R_{\Sigma} = R_{SWIR} + R_{red}$, $R_{\Delta} = R_{SWIR} - R_{red}$]. The Vegetation Condition Albedo Drought Index (VCADI, Ghulam et al., 2007d) is derived from the broadband albedo, α (reflectance spectrum integrated from 700 to 4000 nm), that is inversely related to soil moisture.

The existing optical indices (Table 1) are mostly empirical, lacking the physical foundation that is at the core of thermal-optical methods such as proposed by Moran et al. (1994) and Carlson et al. (1994). To overcome the TOTRAM limitations as well as the empiricism of optical indices, we propose a novel physically-based trapezoid model, hereinafter termed OPtical TRApezoid Model (OPTRAM), which is based on a recently developed physical relationship between soil moisture and shortwave infrared transformed reflectance, *STR* (Sadeghi et al., 2015). Because OPTRAM does not require thermal RS data it can be directly applied to estimate soil moisture from Sentinel-2 observations. In addition, because *STR* is used instead of *LST*, OPTRAM is hypothesized to only require a single universal parameterization for a given location. In the following, we introduce the theoretical basis of OPTRAM, evaluate the predictive capabilities of the universally parameterized OPTRAM with Sentinel-2 observations, and compare OPTRAM and TOTRAM based on Landsat-8 observations.

2. Theoretical background

2.1. The traditional thermal-optical trapezoid model (TOTRAM)

The traditional trapezoid model, TOTRAM, is based on the pixel distribution within the *LST*-VI space. The most common vegetation index used in TOTRAM is the Normalized Difference Vegetation Index (*NDVI*) given as:

$$NDVI = \frac{R_{NIR} - R_{red}}{R_{NIR} + R_{red}} \quad (1)$$

where R_{NIR} is the near-infrared band reflectance and R_{red} is the red band reflectance. An inverse linear relationship between surface soil moisture (θ) and *LST* is then assumed:

$$W = \frac{\theta - \theta_d}{\theta_w - \theta_d} = \frac{LST_d - LST}{LST_d - LST_w} \quad (2)$$

where W is the soil moisture content normalized by the local minimum dry soil moisture content, θ_d , and the local maximum wet soil moisture content, θ_w . The LST_d and LST_w terms are the *LSTs* of the dry and wet soil,

Table 1
Soil moisture and drought indices derived from optical RS observations.

Index	Reference	Relationship ^a
Shortwave Infrared Water Stress Index, <i>SIWSI</i>	Fensholt and Sandholt (2003)	$SIWSI = \frac{R_{SWIR} - R_{NIR}}{R_{SWIR} + R_{NIR}}$
Ecological Safety Monitoring Index, <i>ESMI</i>	Ghulam et al. (2004)	$ESMI = \frac{NDVI}{\alpha}$
Perpendicular Drought Index, <i>PDI</i>	Ghulam et al. (2007a)	$PDI = \frac{R_{red} + MR_{NIR}}{\sqrt{1+M^2}}$
Modified Perpendicular Drought Index, <i>MPDI</i>	Ghulam et al. (2007b)	$MPDI = \frac{PDI - f_v PDI_v}{1-f_v}$
Shortwave-infrared Perpendicular Drought Index, <i>SPDI</i>	Ghulam et al. (2007c)	$SPDI = \frac{R_{SWIR} + MR_{NIR}}{\sqrt{1+M^2}}$
Vegetation Condition Albedo Drought Index, <i>VCADI</i>	Ghulam et al. (2007d)	$VCADI = \frac{\alpha - i_w - s_w NDVI}{i_d - i_w + (s_d - s_w) NDVI}$
Distance Drought Index, <i>DDI</i>	Qin et al. (2010)	$DDI = \frac{\sqrt{R_{red}^2 + R_{NIR}^2}}{1+NDVI}$
Modified Shortwave-infrared Perpendicular Drought Index, <i>MSPDI</i>	Feng et al. (2013)	$MSPDI = \frac{R_{\Sigma} + MR_{\Delta}}{\sqrt{1+M^2}}$
Visible and Shortwave-infrared Drought Index, <i>VSDI</i>	Zhang et al. (2013)	$VSDI = 1 - (R_{SWIR} + R_{red} - 2R_{blue})$
Triangle Soil Moisture Index, <i>TSMI</i>	Amani et al. (2016)	$TSMI = c_0 + \sum_{i=1}^{10} c_i p_i$

^a R_{red} , R_{blue} , R_{NIR} and R_{SWIR} : reflectance for red, blue, NIR and SWIR bands, respectively; α : broadband albedo; $NDVI$: normalized difference vegetation index, Eq. (1), $R_{\Sigma} = R_{SWIR} + R_{red}$, $R_{\Delta} = R_{SWIR} - R_{red}$; M : slope of the soil line in the $R_{red} - R_{NIR}$ or $R_{SWIR} - R_{NIR}$ or $R_{\Sigma} - R_{\Delta}$ space; f_v : fractional vegetation cover; PDI_v : *PDI* of sole vegetation; i_d and s_d : intercept and slope of the dry edge in the $\alpha - NDVI$ space, respectively; i_w and s_w : intercept and slope of the wet edge in the $\alpha - NDVI$ space, respectively; p_i ($i = 1$ to 10): either a distance or an angle associated with the location of a random pixel in the $R_{red} - R_{NIR}$ space; c_i : regression coefficient of p_i .

respectively, where LST_d and LST_w are obtained from the LST - $NDVI$ trapezoid (Fig. 1) for a specific location (satellite scene). The upper (dry) and lower (wet) edges of the trapezoid are used to solve for LST_d and LST_w at any given $NDVI$ (i.e., fractional vegetation cover):

$$LST_d = i_d + s_d NDVI \quad (3)$$

$$LST_w = i_w + s_w NDVI \quad (4)$$

Combining Eqs. (2), (3) and (4), the soil moisture for each pixel can be estimated as a function of LST and $NDVI$:

$$W = \frac{i_d + s_d NDVI - LST}{i_d - i_w + (s_d - s_w) NDVI} \quad (5)$$

2.2. The new optical trapezoid model (OPTRAM)

The new trapezoid model, OPTRAM, is based on the idea of replacing LST in TOTRAM with a measure for soil moisture in the optical domain. Based on the Kubelka and Munk (1931) two-flux radiative transfer model, Sadeghi et al. (2015) developed a physical model exhibiting a linear relationship between surface moisture content and SWIR transformed reflectance:

$$W = \frac{\theta - \theta_d}{\theta_w - \theta_d} = \frac{STR - STR_d}{STR_w - STR_d} \quad (6)$$

where STR is the SWIR transformed reflectance and STR_d and STR_w are the STR at θ_d and θ_w , respectively. The STR is related to SWIR reflectance, R_{SWIR} , as follows:

$$STR = \frac{(1 - R_{SWIR})^2}{2R_{SWIR}} \quad (7)$$

The previously derived Eq. (6) has been tested for bare soils for two SWIR bands (i.e., 1650 nm corresponding to band 6 of Landsat 8, and 2210 nm corresponding to band 7 of Landsat 8), and it has been demonstrated that the model is highly accurate, especially at 2210 nm. Eq. (6) was also derived for vegetated soils based on the Kubelka and Munk radiative transfer model and holds for any fractional vegetation cover (i.e., any $NDVI$) (see Appendix A). An additional assumption required for this derivation is the linear relationship between soil- and vegetation-water contents.

For vegetated soils, θ in Eq. (6) is assumed to be correlated to root zone soil moisture through the vegetation response to soil moisture deficit in the root zone. This assumption conforms to previous studies (Wang et al., 2007; Crow et al., 2008; Liu et al., 2012; Schnur et al., 2010; Peng et al., 2014; Santos et al., 2014) that have applied remotely

sensed vegetation indices to quantify plant vigor and relate it to root zone soil moisture. The soil moisture status influences the vegetation water status and thereby changes the spectral characteristics of the vegetation (Santos et al., 2014). The extent of the root zone varies depending on plant type and growth stage. For example, for coffee trees, Santos et al. (2014) found the highest correlation between RS-based vegetation indices and soil moisture to be at a depth of 60 cm.

Based on the assumption of a linear relationship between soil- and vegetation-water contents, we expect that the STR - $NDVI$ space forms a trapezoid as well. Therefore, the parameters of Eq. (6) can be obtained for a specific location (e.g., satellite scene) from the dry and wet edges of the optical trapezoid, depicted in Fig. 1:

$$STR_d = i_d + s_d NDVI \quad (8)$$

$$STR_w = i_w + s_w NDVI \quad (9)$$

Combining Eqs. (6), (8) and (9), the soil moisture for each pixel can be estimated as a function of STR and $NDVI$:

$$W = \frac{i_d + s_d NDVI - STR}{i_d - i_w + (s_d - s_w) NDVI} \quad (10)$$

A comparison of Eqs. (5) and (10) reveals that the new OPTRAM is analogues to TOTRAM with the exception that LST is replaced with STR . In contrast to the LST - $NDVI$ space, which varies over time due to variations of ambient atmospheric parameters, we expect the STR - $NDVI$ space to remain nearly time invariant because reflectance is a function of only the surface properties and not the ambient atmospheric conditions. Therefore, we expect feasibility of a universal parameterization of OPTRAM that is valid for all observation dates at a specific location.

It should be noted that the STR - θ relationship is only valid for partially and fully saturated soils, but not for oversaturated soils (i.e. standing surface water). This is because water in excess of saturated soil moisture will still increase STR , but the actual soil moisture, θ , cannot increase beyond the saturated soil moisture content. Therefore, for scenes that include many oversaturated pixels (e.g., conditions after heavy precipitation) the wet edge (saturated edge in this case) falls somewhere below the upper edge of the optical trapezoid (i.e., oversaturated edge in Fig. 1). For this condition, $W = 1$ is assumed for all pixels above the wet edge (i.e., $STR > STR_w$). Carlson (2013) also suggested not to incorporate pixels containing standing water in the TOTRAM trapezoid. However, as shown below, OPTRAM is more sensitive to oversaturated pixels than TOTRAM.

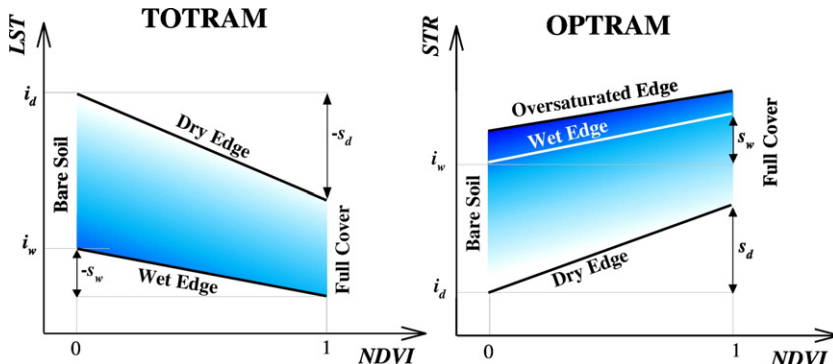


Fig. 1. Sketch illustrating parameters of the traditional thermal-optical trapezoid model [Eq. (5), TOTRAM] and the new optical trapezoid model [Eq. (10), OPTRAM]. TOTRAM and OPTRAM are parameterized based on the pixel distributions within the LST - $NDVI$ space and STR - $NDVI$ space, respectively. $NDVI$ is the normalized difference vegetation index, LST is the land surface temperature, and STR is the SWIR transformed reflectance [see Eq. (7)].

3. Materials and methods

3.1. Test sites and in situ soil moisture data

The newly proposed and traditional trapezoid models, OPTRAM and TOTRAM, were evaluated for the Walnut Gulch (WG) and Little Washita (LW) watersheds in southern Arizona and in southwestern Oklahoma, respectively (Fig. 2). The sites that vastly differ in climatic conditions, surface topology and land cover are among the most densely instrumented watersheds in the world and have previously served as validation sites for microwave remote sensing experiments (Cosh et al., 2006; Jackson et al., 2009, 2012). Soil moisture measured with a network of electromagnetic sensors installed in 5-cm depth were used to evaluate the RS-based surface soil moisture estimates.

3.1.1. Walnut Gulch watershed

The WG watershed is part of the San Pedro river basin and extends over an area of 148 km² covered with shrubs (two thirds) and grassland (one third). The elevation ranges from 1220 to 1933 m above sea level and the diverse topology transitions from very steep slopes ($\geq 50\%$) to nearly flat concave basin floors. The climate is semiarid with an average annual temperature of 17.7 °C and average annual precipitation of 350 mm, commonly falling between April and September. Soils are classified as gravelly and sandy loams with a high percentage of rock and gravel close to the soil surface (Renard et al., 1993). For more detailed information about the WG watershed readers are referred to Keefer et al. (2008).

The WG watershed is densely instrumented with 88 rain gauges, 19 of which are colocated with soil moisture sensors installed at 5-cm depth. Soil moisture data from 15 rain-gauge stations were employed together with 5-cm soil moisture data from the Soil Climate Analysis Network (SCAN) site no. 2026 (Fig. 2) for validation of OPTRAM and TOTRAM moisture estimates. Note that for 4 of the 19 locations no reliable soil moisture measurements were available.

3.1.2. Little Washita watershed

The LW watershed extends over an area of 610 km² dominated by grass and cropland, draining into a tributary of the Washita River. The elevation ranges from 320 to 480 m above sea level with gently to moderately rolling topography. The climate is classified as moist and sub-

humid with an average annual temperature of 16 °C and an average annual precipitation of 750 mm mostly falling in spring and fall. The soil texture ranges from fine sand to silty loam. Hydrological and meteorological measurements have been conducted in the watershed for decades, providing scientists with long-term data for studying soil and water conservation, water quality, and basin hydrology (Starks et al., 2014). The watershed contains the 20-station USDA-ARS Micronet for monitoring spatial and temporal soil moisture dynamics. The 5-cm soil moisture data from 17 Micronet stations (Fig. 2) were used as ground truth for validating OPTRAM and TOTRAM estimates (for 3 stations no reliable soil moisture data were available).

3.2. Satellite data and image analysis

Multispectral ESA Sentinel-2 (S2) and NASA Landsat-8 (L8) satellite images acquired from the ESA Sentinel Scientific Data Hub (URL: <https://scihub.copernicus.eu/dhus/#/home>) and the United States Geological Survey (USGS) Earth Explorer (URL: <https://ers.cr.usgs.gov>) were used in this study. Sentinel-2 incorporates an innovative wide-swath, high spatial (10 to 60-m) and temporal (~10-day) resolution, multispectral imager with 13 spectral bands covering the visible, NIR and SWIR electromagnetic frequency domains. Landsat-8 houses the Operational Land Imager (OLI) and the Thermal Infrared Sensor (TIRS), which image the land surface at 11 spectral bands in the optical and thermal infrared domains with 30- to 100-m spatial resolution and 16-day temporal resolution.

A total of 40 cloud-free level-1C S2 images and level-1 L8 images acquired in 2015 and 2016 were used in this study (Table 2). There were only a limited number of cloud-free S2 images available for the study period, with the earliest dating back to late 2015. Ground truth measurements from the abovementioned soil moisture networks were considered at the imaging times of the L8 and S2 satellites on the dates listed in Table 2. Though only a limited number of images were available, it should be noted that measured soil moisture values varied over the full range from dry to saturated, allowing for extensive validation of OPTRAM and TOTRAM.

Flowcharts illustrating the sequence of S2 and L8 data analyses steps for mapping surface soil moisture with OPTRAM and TOTRAM are depicted in Fig. 3. Image radiometric calibration was first performed to convert the pixel digital numbers, DN, to the top-of-atmosphere (TOA)

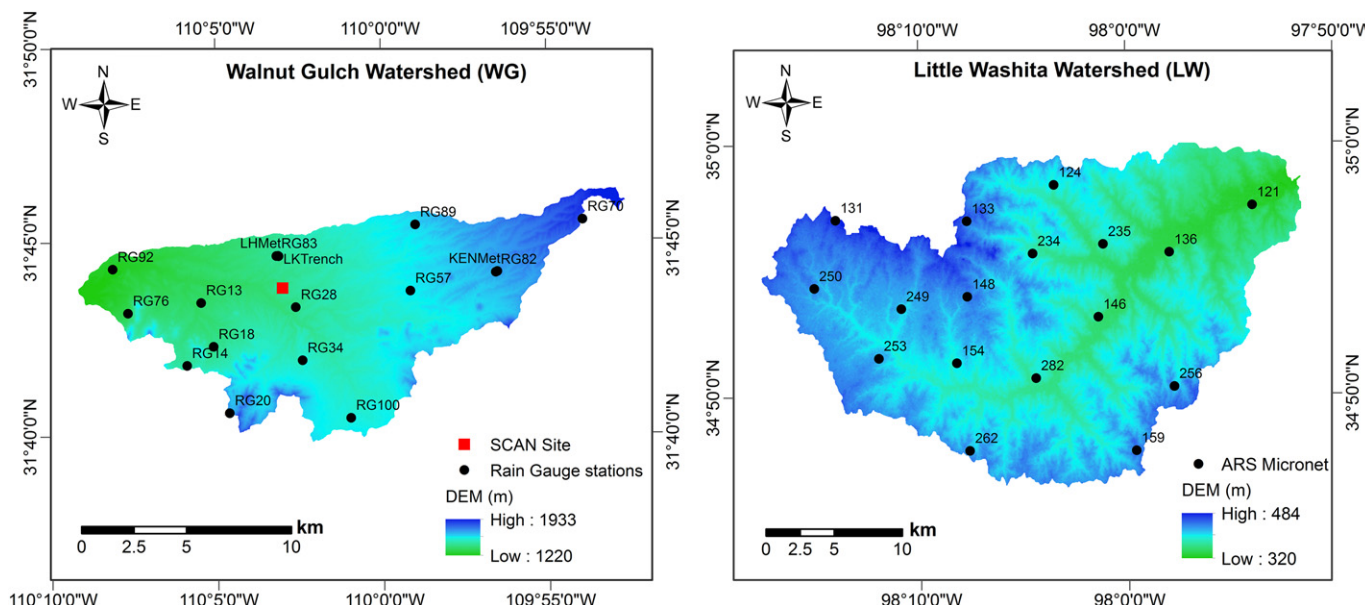


Fig. 2. The Walnut Gulch and Little Washita watersheds with marked locations of soil moisture sensors used for validation of OPTRAM and TOTRAM. Note that the sensor installation depth is 5 cm.

Table 2

Satellite images used in this study.

Satellite	Watershed	No. of images	Acquisition date
Sentinel-2	WG	17	2015 (Dec. 2, Dec. 9); 2016 (Jan. 5, Jan. 11, Jan. 21, Feb. 7, Feb. 10, Mar. 21, Apr. 20, Apr. 30, May 10, May 17, May 20, May 30, Jun. 6, Jun. 19)
Sentinel-2	LW	4	2016 (Feb. 15, Mar. 16, May 5, Jun. 14)
Landsat-8	WG	12	2015 (Nov. 1, Nov. 17, Dec. 3); 2016 (Jan. 20, Feb. 5, Feb. 21, Mar. 24, Apr. 9, Apr. 25, May 11, May 27, Jun. 12)
Landsat-8	LW	5	2015 (Dec. 2, Dec. 18); 2016 (Feb. 4, Mar. 23, May 11)

reflectance values. For the S2 level-1C images a simple scaling factor of 0.0001 was applied and for the L8 images the following equation was used ([USGS, 2016](#)):

$$R_{TOA} = \frac{A_B + M_B DN}{\sin \varphi_s} \quad (11)$$

where R_{TOA} is the TOA reflectance, A_B and M_B are the band-specific additive and multiplicative rescaling factors, respectively, and φ_s is the local sun elevation angle, which is extracted from the image metadata file. Atmospheric corrections were applied to the satellite images to convert TOA reflectance to bottom-of-atmosphere (or surface) reflectance using the Fast Line-of-sight Atmospheric Analysis of Hypercubes (FLAASH) atmospheric correction tool in ENVI 5.3 and the Semi-automatic Classification Plugin (SCP) in QGIS ([USGS, 2016](#); [Stratoulias et al., 2015](#)). The images were projected into WGS84 UTM Zones 12 and 14 North.

Various indices and algorithms are available to delineate water bodies and wetlands in satellite images. Both supervised and unsupervised multispectral classification of optical remote sensing data have been successfully applied to delineate water boundaries ([Kingsford et al., 1997](#); [Frazier and Page, 2000](#); [Xie et al., 2016](#)). Here we simply applied an iso-cluster unsupervised classification scheme for detecting and

masking surface water bodies using combined visible, NIR and SWIR bands. Excellent agreement was found between this method and the approach proposed in [Feyisa et al. \(2014\)](#) based on the “Automated Water Extraction Index” [their Eqs. (2) and (3)], which was later employed to check the accuracy of the classification method. The image analysis operations were performed with the ArcGIS 10.3 (Esri, Redlands, CA), ENVI 5.3 (Harris Corp., Broomfield, CO), QGIS 2.8.9 (QGIS Development Team, 2016), and MATLAB R2015b (MathWorks Inc, Natick, MA) software packages.

Reflectance at the red band [S2 band 4 (665 nm), L8 band 4 (665 nm)] and NIR band [S2 band 8 (842 nm), L8 band 5 (865 nm)] were used to calculate the NDVI [Eq. (1)]. Reflectance at the SWIR band [S2 band 12 (2190 nm), L8 band 7 (2200 nm)] was used for calculation of the STR [Eq. (7)] following the [Sadeghi et al. \(2015\)](#) analyses. The S2 band 12 images with 20-m spatial resolution were resampled to 10-m resolution with the nearest neighbor method to match the spatial resolutions of bands 4 and 8.

Land surface temperature (LST) was calculated from the L8 thermal infrared data (L8 bands 10 and 11) according to the L8 data user handbook ([USGS, 2016](#)). First, spectral radiance was converted to brightness temperature, T_b , based on Planck's radiance function, where the average of bands 10 and 11 were used. Note that almost identical results were obtained when only band 10 was employed. This check was performed

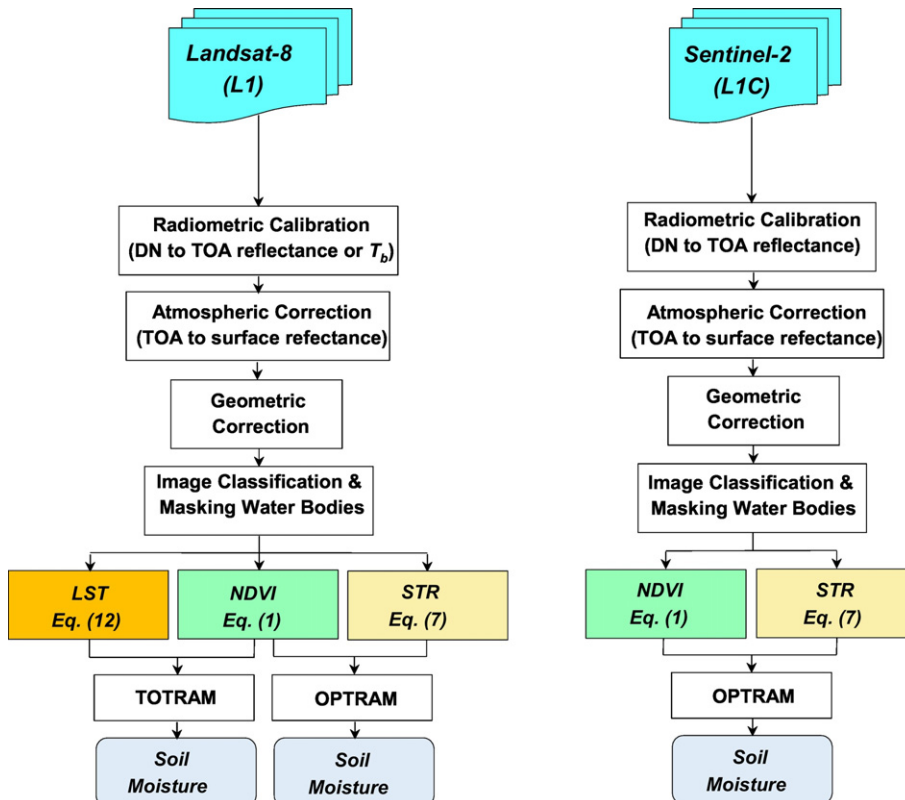


Fig. 3. Flowcharts illustrating the sequence of Sentinel-2 and Landsat-8 data analyses steps for mapping surface soil moisture with TOTRAM, Eq. (5), and OPTRAM, Eq. (10).

to see if there is any effect of band selection. Then LST was determined from T_b using a single channel algorithm (Qin et al., 2001), given as:

$$LST = \{a(1-c-d) + [b(1-c-d) + c + d]T_b - dT_a\}/c \quad (12)$$

where T_a is the effective atmospheric temperature, a and b are coefficients of a linear function to approximate the derivative of the Planck radiance function for the thermal band [see Eqs. (16) and (22) of Qin et al. (2001)] and c and d are defined as:

$$c = \varepsilon\tau \quad (13)$$

$$d = (1-\tau)[1 + (1-\varepsilon)\tau] \quad (14)$$

where ε is the ground emissivity and τ is the atmospheric transmittance.

The coefficients a and b were determined based on Table 1 of Wang et al. (2015), T_a was obtained from Eq. (32) of Qin et al. (2001) as a function of near surface air temperature (i.e. meteorological station data), ε was estimated as a function of $NDVI$, as proposed by Van De Griend and Owe (1993) and Zhang et al. (2006), and τ was determined from local water vapor content data based on Table 6 of Wang et al. (2015). Water vapor content was obtained from near surface air temperature and relative humidity data from meteorological stations located within the WG and LW watersheds.

3.3. Model parameterization

TOTRAM [Eq. (5)] and OPTRAM [Eq. (10)] were parameterized based on the pixel distribution within the $LST-NDVI$ space and $STR-NDVI$ space, respectively. Two different scenarios were considered for determining parameters of Eqs. (5) and (10) as explained below. To test whether TOTRAM and OPTRAM could be universally parameterized, we used

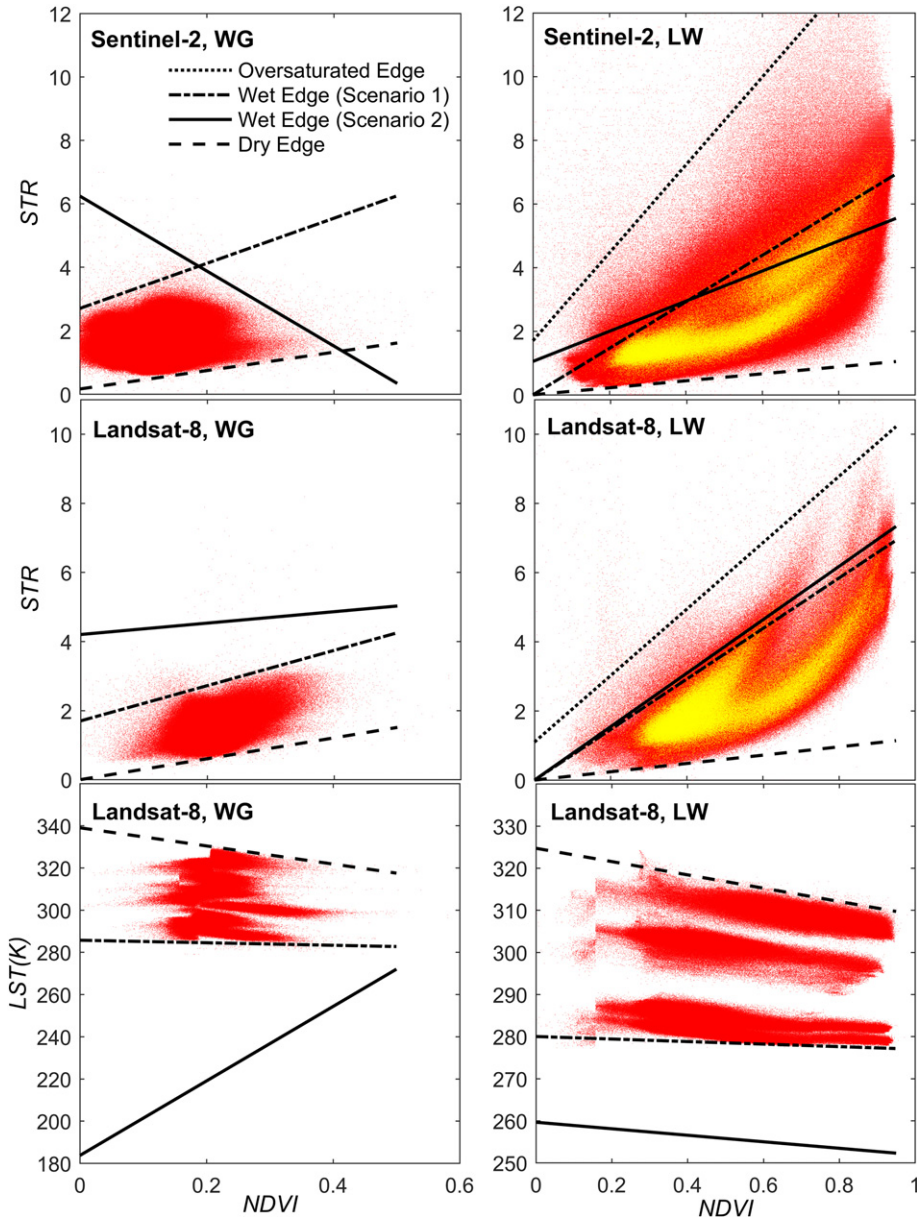


Fig. 4. Pixel distributions within the $STR-NDVI$ (OPTRAM) and $LST-NDVI$ (TOTRAM) spaces for all images listed in Table 2 (red dots). The yellow dots shown for the optical trapezoids in the Little Washita watershed are from the images resampled to 120-m resolution and were used to determine the wet edge, which falls below the upper edge for this case due to the existence of oversaturated pixels. Thermal imaging required by TOTRAM is not available on the Sentinel-2 satellite.

Table 3

TOTRAM [Eq. (5)] and OPTRAM [Eq. (10)] parameters obtained for the Walnut Gulch (WG) and Little Washita (LW) watersheds based on Sentinel-2 (S2) and Landsat-8 (L8) satellite data.

Model, sensor, area	Dry edge		Wet edge (scenario 1)		Wet edge (scenario 2)		Oversaturated edge	
	i_d	s_d	i_w	s_w	i_w	s_w	i_{os}	s_{os}
OPTRAM, S2, WG	0.16	2.90	2.70	7.10	6.24	-11.81	-	-
OPTRAM, S2, LW	0.00	1.10	0.00	7.30	1.05	4.73	1.70	13.80
OPTRAM, L8, WG	0.00	2.65	1.70	5.10	4.20	1.65	-	-
OPTRAM, L8, LW	0.00	1.20	0.00	7.30	0.00	7.72	1.10	9.60
TOTRAM, L8, WG	339.0	-43.0	285.7	-6.0	183.7	176.6	-	-
TOTRAM, L8, LW	324.7	-15.8	280.0	-3.0	259.6	-7.7	-	-

one integrated trapezoid incorporating pixel distributions from all available images for each scenario and watershed.

3.3.1. Scenario 1

For the first scenario, dry (i_d and s_d) and wet (i_w and s_w) edges were determined by visual inspection of the *LST-NDVI* or *STR-NDVI* spaces so that the trapezoids surrounded the majority of the pixels. Visual matching was preferred over least-square regression in order to omit points associated with oversaturated or shadowed pixels scattered around the main point cloud of each trapezoid. Carlson (2013) also suggested that the edges can be best defined by “visual inspection” of the pixel distributions.

From i_d and s_d (dry edge parameters) and i_w and s_w (wet edge parameters), the normalized moisture content, W , was estimated for each pixel with Eqs. (5) and (10). To compare soil moisture estimates with the in situ measured data, values of W at pixels containing in situ sensors

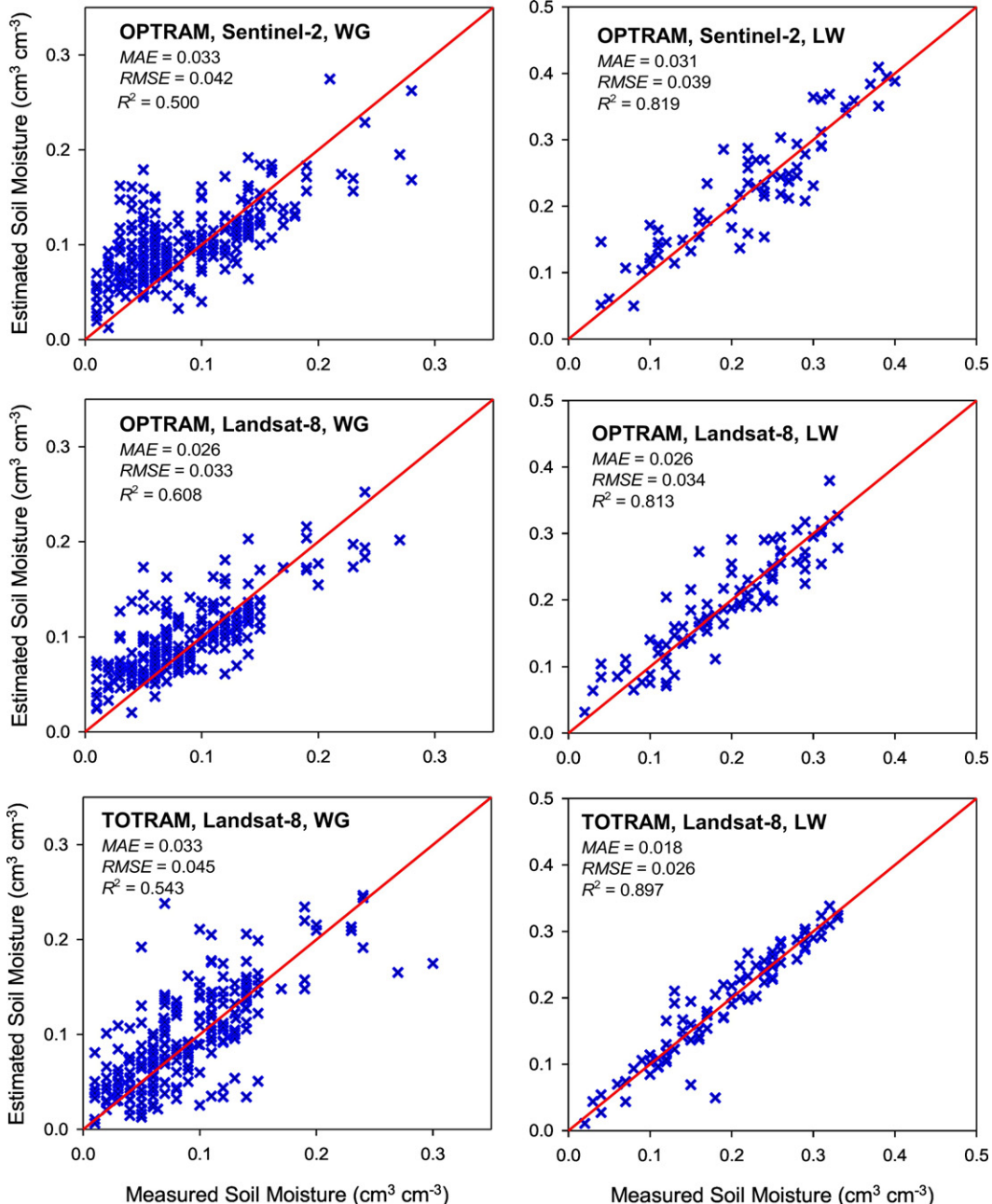


Fig. 5. OPTRAM and TOTRAM soil moisture estimates (parameterized based on scenario 1) compared to in situ soil moisture measurements for the Walnut Gulch (WG) and Little Washita (LW) watersheds.

were converted to soil water content, θ . Values of θ_d and θ_w were assumed to be constant for each site during the study period. The values were obtained via linear regression analysis of RS-based W data and in situ measured θ data.

From the resultant optical trapezoids for the LW watershed, it was apparent that the image classification in LW was only able to remove deep surface water bodies, but not shallow water ponds. Hence, the fitted upper edge in this case was the oversaturated edge shown in Fig. 1 and not the wet edge. It was observed that the oversaturated zone within the trapezoid was significantly thicker for the Sentinel-2 data than for the Landsat-8 data. This can be attributed to the spatial resolution difference (i.e., the coarser the resolution, the lower the chance of an entire pixel to be oversaturated due to shallow surface ponds). Inspired by this result, we resampled both S2 and L8 images to a coarser resolution using the ArcGIS software package to solve for the wet edge in the LW watershed optical trapezoid. We empirically found that a

resolution of 120 m for both S2 and L8 images provided reasonable wet edges. Note that the resampled images were only used to determine the wet edge in scenario 1. All other calculations for estimating soil moisture were performed using the original pixel sizes, assuming $W = 1$ for any point above the wet edge.

3.3.2. Scenario 2

Although W maps of scenario 1 were independent from in situ data, the estimated θ at the stations were dependent on calibrations using in situ data. Hence, a second parameterization scenario was established to examine the validity of the physical basis of TOTRAM and OPTRAM, or in other words, the strength of the correlation between θ and LST in TOTRAM [i.e. validity of Eq. (2)] and that of θ and STR in OPTRAM [i.e. validity of Eq. (6)] at a given $NDVI$. For scenario 2, all in situ measured θ values were normalized based on in situ measured θ_d and θ_w (i.e., minimum and maximum measured θ at each station during 2015 and

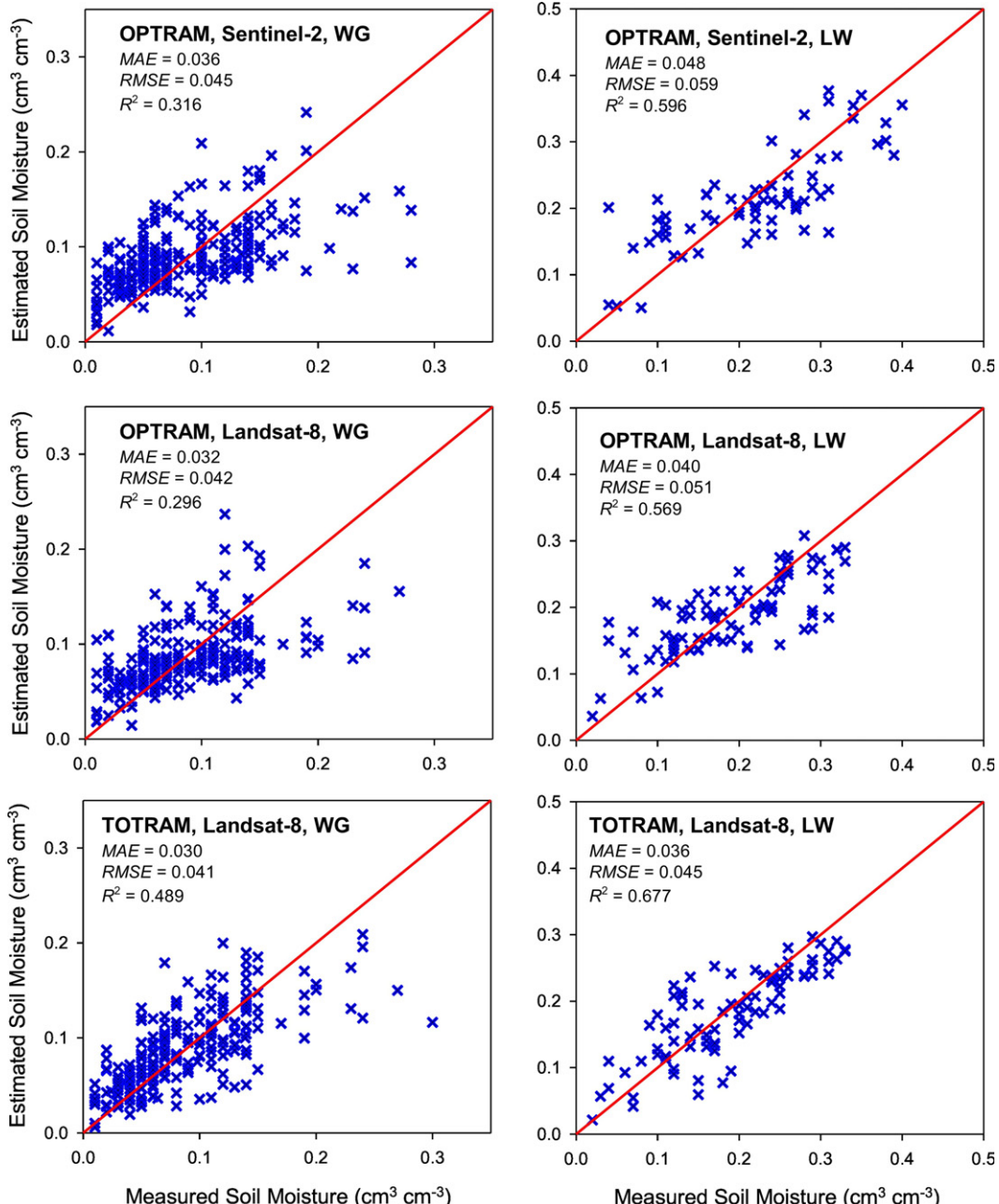


Fig. 6. OPTRAM and TOTRAM soil moisture estimates (parameterized based on scenario 2) compared to in situ soil moisture measurements for the Walnut Gulch (WG) and Little Washita (LW) watersheds.

2016). This way, a set of reference W values, hereinafter referred to as “measured W ”, were obtained to evaluate estimated W values with the two models. Then the wet edge (i_w and s_w) was determined via least-square regression of Eqs. (5) and (10) to $W(LST, NDVI)$ or $W(STR, NDVI)$ data, while the dry edge (i_d and s_d) was kept the same as in scenario 1. Estimated and measured W values were also converted back to θ values based on the in situ measured θ_d and θ_w at each station to compare the models accuracy in terms of θ as well.

4. Results and discussion

4.1. Model parameters

Pixel distributions within the $STR-NDVI$ and $LST-NDVI$ space for all images listed in Table 2 are depicted in Fig. 4. Corresponding model parameters are listed in Table 3. The following is evident from Fig. 4:

- (i) A nearly trapezoidal shape is formed by the pixels in the $STR-NDVI$ space in most cases, although the edges are not perfectly linear. This primarily verifies our hypothesis that soil moisture is highly correlated to STR even in densely vegetated soils (e.g. $NDVI > 0.6$).
- (ii) In both the WG and LW watersheds, the S2-based and L8-based trapezoids are generally similar in shape [e.g., as evident from comparison of the resampled S2 and L8 data for the LW watershed (yellow trapezoids) or from OPTRAM's wet edge parameters for LW in scenario 1]. This similarity leads to the conclusion that universal parameterization of OPTRAM is achievable because S2 and L8 data were acquired on different dates (Table 2).
- (iii) The wet edge in both OPTRAM and TOTRAM in WG varies

significantly between scenarios 1 and 2. In contrast to scenario 1, the OPTRAM model parameterization for scenario 2 is different between S2 and L8 data (Table 3). For example, for S2 in WG, scenario 1 led to a positively-sloped wet edge, while scenario 2 led to a negatively-sloped wet edge yielding a triangular geometry. This difference implies that the least-square model parameterization (scenario 2) does not necessarily lead to the physically-based theoretical dry and wet edges, which one may obtain from radiative transfer modeling. In the WG watershed, the TOTRAM wet edge in scenario 2 is too far away from the wet edge in scenario 1. This discrepancy is obviously due to the fact that θ values at the time of L8 passage were well below the maximum θ values measured at the stations during the entire study period (2015 and 2016), which were considered in scenario 2.

- (iv) The integrated $LST-NDVI$ trapezoid used to parameterize TOTRAM consists of several separate smaller trapezoids each corresponding to a specific date. This is because the LST depends on ambient environmental factors besides soil moisture and implies that universal parameterization of TOTRAM is not possible. This behavior was not observed for OPTRAM.

4.2. Overall accuracy

A comparison of OPTRAM and TOTRAM soil moisture estimates for scenario 1 parameterization with in situ measured 5-cm moisture data is depicted in Fig. 5. The results indicate that calibration of both models with in situ data generally leads to reasonable soil moisture estimates ($\leq 0.04 \text{ cm}^3 \text{ cm}^{-3}$ error). Overall, similar accuracy was achieved for

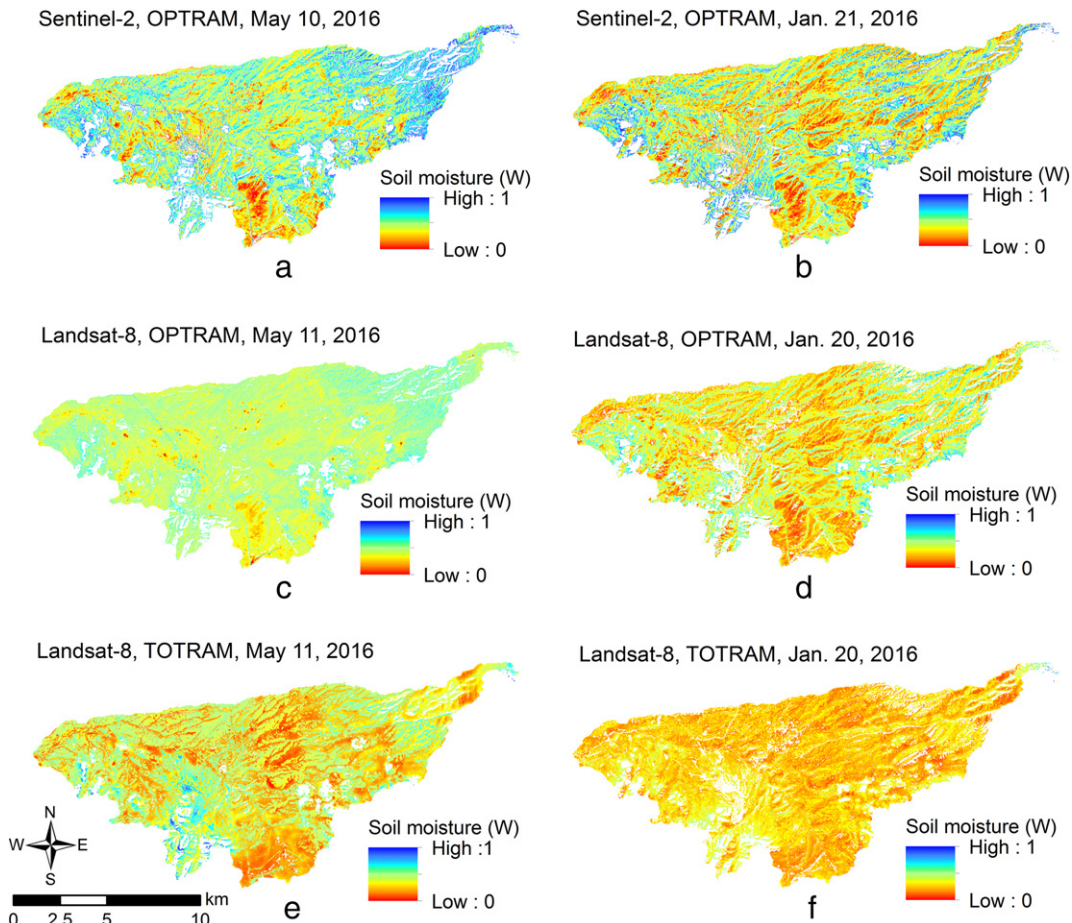


Fig. 7. Soil moisture maps generated with OPTRAM and TOTRAM based on scenario 2 parameterization for the Walnut Gulch watershed. White pixels represent masked pixels due to water bodies, shadows, and rural/urban areas.

both models. OPTRAM performed slightly better for WG, whereas the accuracy of TOTRAM was slightly better for LW.

The moisture estimations are generally better for the LW watershed. Existence of more sparsely vegetated and bare soils in WG could lead to lower TOTRAM accuracy, due to the fact that the $LST-\theta$ relationship is generally nonlinear for bare soils (Aminzadeh and Or, 2013; Janatian et al., 2017). Also existence of larger areas of bare land in WG could affect both TOTRAM and OPTRAM accuracy due to the discrepancy between what these models estimate in bare land (i.e. 0-cm soil moisture) and what was measured (i.e. 5-cm soil moisture). A significant difference between 0-cm and 5-cm soil moisture is expected based on simulations using Richards' equation (e.g. Sadeghi et al., 2017).

Another simple and perhaps more important reason for higher accuracy of both models in LW could be the smaller number of analyzed images (i.e. less data for each station to fit a line) concurrent with the wider range of soil moisture variations. This in conjunction with the local calibration (i.e. scenario 1) of estimated W potentially leads to better fits for any case. Hence, estimates of models without local calibration (i.e. scenario 2) such as those presented in Fig. 6 will reveal more about robustness of the models.

Measured and estimated θ from scenario 2 are compared in Fig. 6. Although the estimation errors increased when compared to scenario 1, they remained within $\sim 0.04\text{--}0.05\text{ cm}^3\text{ cm}^{-3}$, which is considered a

reasonable accuracy for RS and large-scale mapping of soil moisture (Entekhabi et al., 2014). Considering that no in situ calibration was performed for scenario 2, the obtained reasonable accuracy reveals that the underlying assumptions of OPTRAM and TOTRAM are generally valid under natural conditions. Specifically, the existence of high correlations between θ and LST for TOTRAM and between θ and STR for OPTRAM are verified.

In addition to linear relationships of θ with LST and STR , linear dry and wet edges were assumed in both models. In other words, at the same soil moisture level, linear relationships between STR and $NDVI$ in OPTRAM and between LST and $NDVI$ in TOTRAM were assumed. These relationships are also not exact, as evident from Fig. 4. Previous studies (e.g., Mallick et al., 2009) evaluated both linear and nonlinear edges in TOTRAM. The same evaluation is needed in future studies for OPTRAM, specifically, to evaluate to what extent consideration of more complex edges can improve model accuracy and if this consideration does not compromise universal parameterization.

There are certainly more error sources contributing to the data scattering observed in Fig. 6. As discussed above, the discrepancy between the sensing and measurement depths, especially in bare soils, is one source of error. Effects of the ambient environmental conditions on LST in TOTRAM and effects of shadows due to surface roughness on STR in OPTRAM are other potential error sources.

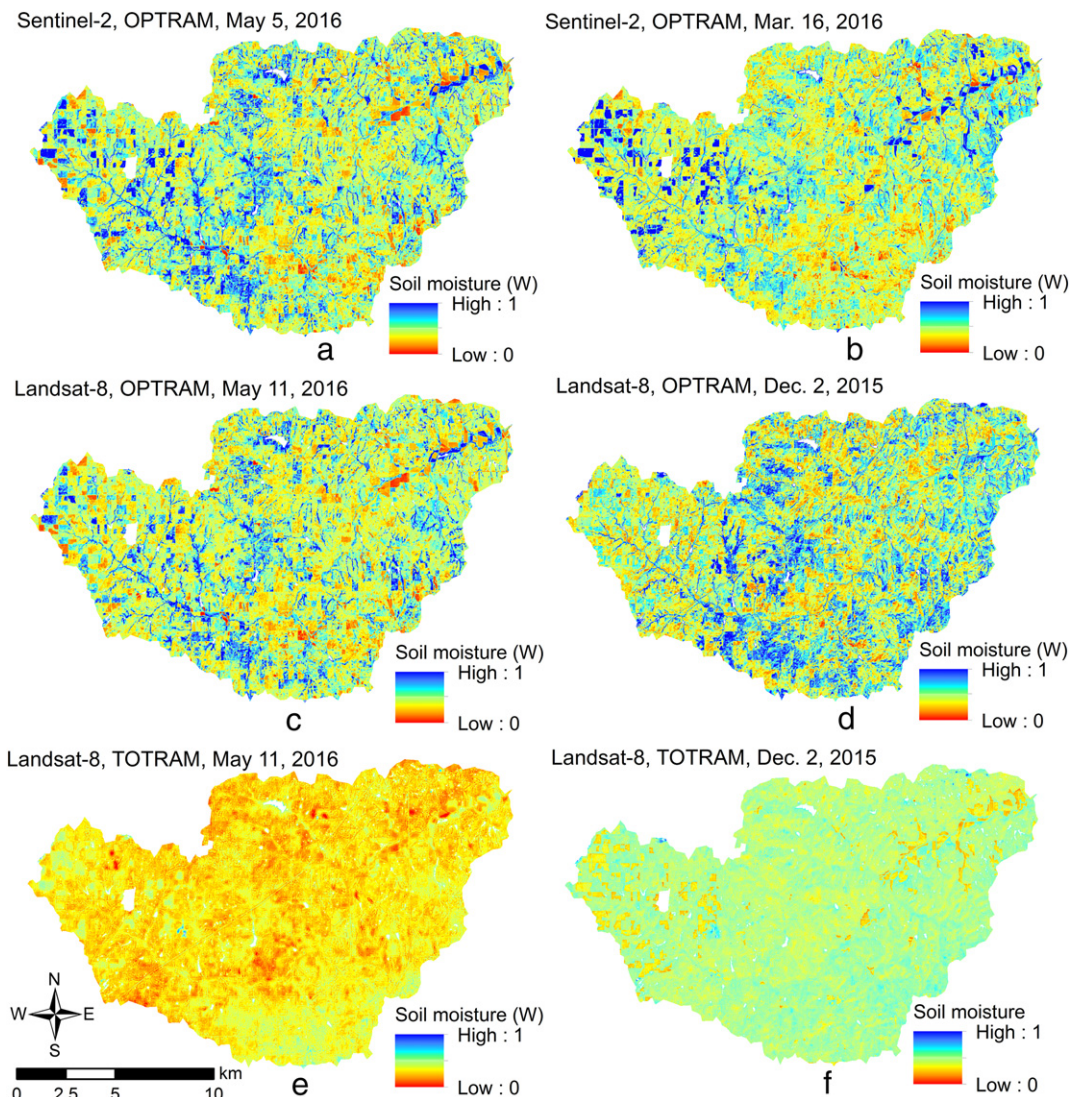


Fig. 8. Soil moisture maps generated with OPTRAM and TOTRAM based on scenario 2 parameterization for the Little Washita watershed. White pixels represent masked pixels due to water bodies, shadows, and rural/urban areas.

4.3. Soil moisture maps

Sample surface soil moisture maps generated from OPTRAM and TOTRAM for scenario 2 parameterization are shown in Figs. 7 and 8. While for the LW watershed the maps obtained from Sentinel-2 and Landsat-8 data are similar, they differ for the WG watershed. The reason is the significant difference of the wet edge between the WG Sentinel-2 and Landsat-8 trapezoids (see Fig. 4 and Table 3). Soil moisture maps generated based on scenario 1 (not shown here) were similar for both WG and LW, because of the similarity of the dry and wet edges.

Although TOTRAM and OPTRAM yielded similar overall accuracy (Figs. 5 and 6), they resulted in substantially different soil moisture maps, especially for the LW watershed. According to the topography of the study areas (Fig. 2), the OPTRAM-based maps look more reasonable. For example, the surface water network evident in Fig. 2 is present in the OPTRAM-based maps, as they show saturation and near saturation values at these pixels. In contrast, TOTRAM resulted in a narrow range of soil moisture in the map in most cases, and hence, the TOTRAM-based maps do not present the surface water network. This fact obviously indicates that universal parameterization of TOTRAM

(i.e. for all dates concurrently) was not successful. To show this more clearly, a date-by-date comparison of the pixel values (estimated W) with measured W at the stations is depicted in Fig. 9.

Fig. 9 clearly indicates that TOTRAM mostly yielded W in a very narrow range (close to average) for each date, while the measured W throughout the watersheds experienced a large degree of spatial variability. This is obviously due to the fact that temporal variability of LST has been significantly larger than its spatial variability, leading to successful prediction of the average soil moisture at each date, but failure in predicting the spatial variability of soil moisture by TOTRAM. In contrast, OPTRAM was able to successfully generate the spatial variability of soil moisture, although its accuracy in predicting the absolute value of soil moisture needs to be viewed with caution.

Date-by-date comparison of the models shown in Fig. 9 reveals that the RMSE of TOTRAM is slightly better than for OPTRAM in most cases (Note that the RMSE values in Fig. 9 are higher than those in Fig. 6, mainly due to different scaling). As discussed, this is because TOTRAM was able to capture temporal variation of the average soil moisture in the watershed, but failed in capturing the detailed spatial variability of soil moisture. The former indicates the strong relationship between θ and

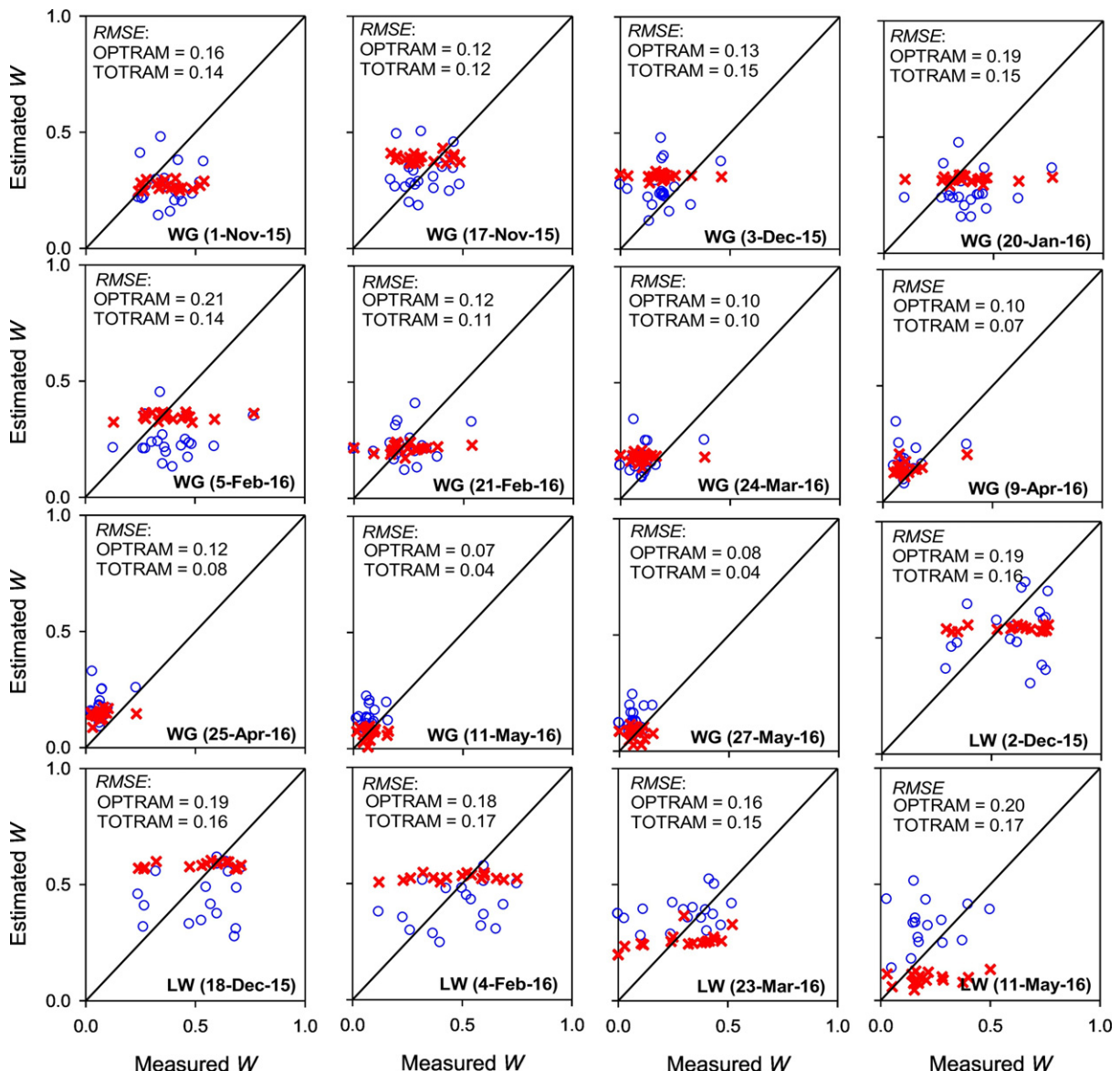


Fig. 9. Estimated versus measured normalized soil moisture [$W = (\theta - \theta_d) / (\theta_w - \theta_d)$] from OPTRAM (blue circles) and TOTRAM (red xs) parameterized based on scenario 2 for Landsat-8 imagery at various dates during 2015 and 2016.

LST and the latter highlights the time-dependence of this relationship due to the change in ambient atmospheric parameters. Therefore, from Figs. 7, 8 and 9, we can conclude feasibility of a universal calibration for the OPTRAM, but not for TOTRAM. In other words, OPTRAM can resolve both of the main limitations of TOTRAM as discussed in the introduction.

4.4. Other optical models

It has been indicated that the two abovementioned inherent limitations of TOTRAM can be resolved when using an optical model, whether it be the model proposed in this paper (OPTRAM) or any of the optical models listed in Table 1. However, it should be stated that OPTRAM is a physically-based model that stands out from all existing empirical optical models. To highlight the advantage of a physically-based optical model over empirical approaches, we compare the performance of OPTRAM with the empirical VCADI model (Ghulam et al., 2007d), which is the most similar model to OPTRAM among those listed in Table 1. The VCADI model is a dryness index bound between 0 and 1 (0 for fully wet and 1 for fully dry conditions). For the sake of consistency with TOTRAM and OPTRAM, we define a corresponding normalized soil moisture, W , as follows:

$$W = \frac{\theta - \theta_d}{\theta_w - \theta_d} = 1 - \text{VCADI} = \frac{i_d + s_d \text{NDVI} - \alpha}{i_d - i_w + (s_d - s_w) \text{NDVI}} \quad (15)$$

Eq. (15) is similar to both Eqs. (5) (TOTRAM) and (10) (OPTRAM), while *LST* in TOTRAM or *STR* in OPTRAM is replaced with the broadband albedo (α). To calculate VCADI, Ghulam et al. (2007d) calculated α in 3

domains, namely, visible (0.4–0.7 μm), NIR (0.7–4 μm) and whole shortwave (0.4–4 μm), applying algorithms developed by Liang (2000). We considered the whole shortwave domain [α_{short} in Eq. (11) of Liang (2000)] in this analysis and only considered the L8 images for the LW watershed.

The pixel distribution within the α -NDVI space is shown in Fig. 10. The presented dry and wet edges were determined considering four different scenarios; (i) both edges were determined visually (similar to scenario 1 described above); (ii) the dry edge was determined visually and the wet edge was determined with least-square regression (similar to scenario 2 described above); (iii) the wet edge was determined visually and the dry edge was determined with least-square regression; (iv) both edges were determined with least-square regression. The model performance corresponding to these four scenarios is shown in Fig. 11.

We found that none of the scenarios led to reasonable matches between the α -NDVI trapezoid model and the actual data. As observed, the dry edge in the α -NDVI space is nearly quadratic rather than linear, leading to a geometry distinctively different than a trapezoid. In scenario 1, both the edges (Fig. 10) and the soil moisture estimates (Fig. 11) are reasonable, but obtained θ_d values were significantly larger than θ_w values at several stations, which is not consistent with the physics of the problem. In scenarios 2 and 4, the soil moisture estimates are reasonable, but the wet and dry edges do not match with the actual pixel distribution. In scenario 3, a reasonable wet edge was obtained via least-square regression, but the accuracy of the soil moisture estimates is low. These results imply that the α -NDVI trapezoid model is not in good agreement with the physical phenomena affecting the soil moisture-reflectance relationship, although it might yield reasonable estimates of soil moisture in some cases.

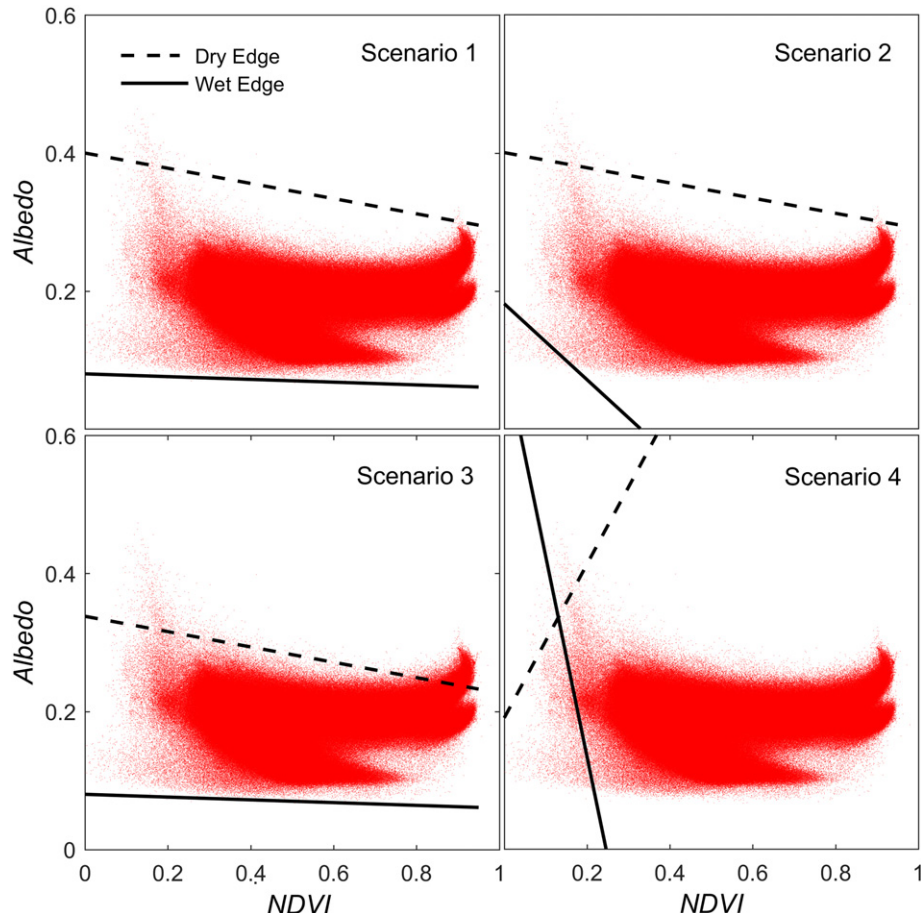


Fig. 10. Pixel distributions within the Albedo-NDVI space for Landsat-8 images from the Little Washita watershed from the dates listed in Table 2. Four different scenarios were considered to determine the edges; (1) both edges determined visually; (2) dry edge determined visually and wet edge determined with least-square regression; (3) wet edge determined visually and dry edge determined with least-square regression; (4) both edges determined with least-square regression.

One noticeable point in the α -NDVI trapezoid is that there is significantly less scattering around the edges when compared to the STR-NDVI trapezoid. This point is considered as an advantage of the α -NDVI trapezoid model when compared to OPTRAM, as the oversaturated pixels are not an issue in this model.

5. Conclusions and future research needs

5.1. Conclusions

The new OPtical TRApeZoid Model (OPTRAM) proposed in this study offers a novel approach to satellite-based remote sensing of soil moisture. OPTRAM has been derived based on the linear physically-based relationship between STR and surface or root-zone soil moisture in bare or vegetated soils [i.e., Eq. (6), derived from a radiative transfer model]. OPTRAM parameters for a given area can be determined either based on the pixel distribution within the STR-NDVI space (scenario 1) or with least-square regression of the model to field observations (scenario 2). The achievable prediction accuracy of OPTRAM is comparable with the accuracy of the conventional trapezoid model (TOTRAM) which utilizes coupled LST-NDVI data. The advantage of the OPTRAM over the TOTRAM is two-fold:

- (i) OPTRAM does not require thermal data, hence, it is applicable to satellites providing only optical data such as the ESA Sentinel-2 satellite.
- (ii) OPTRAM can be universally parameterized for a given location because the STR-soil moisture relationship is not affected by ambient environmental factors (e.g. air temperature, wind speed).

The disadvantage of OPTRAM when compared to TOTRAM is its higher sensitivity to oversaturated and shadowed pixels. When the optical trapezoid consists of too many oversaturated pixels, solving for the wet edge needs some refinements. This, however, may not be a significant limitation because of the feasibility of a single universal model parameterization.

5.2. Future research needs

The concept of the new optical trapezoid model OPTRAM has been introduced in this first paper. However, several remaining issues warrant additional research. In the following, we list some thoughts for further development of OPTRAM:

- (i) Applying OPTRAM for different regions of the world will shed more light on a potential opportunity for universal parameterization. Derivation of theoretical trapezoid edges from laboratory observations or radiative transfer simulations of reflectance of the endmembers (soil, vegetation, etc.) may prove to be effective approaches to universal parameterization of OPTRAM.
- (ii) The spatiotemporal scaling effects on OPTRAM accuracy imposed by utilizing different satellites (e.g., Sentinel, Landsat, and MODIS) need to be further clarified. Because Sentinel-2 was launched not too long ago in the middle of 2015, the time period of this study has been limited to a few months in 2015 and 2016. Evaluation of OPTRAM for longer periods to obtain a robust universal parameterization especially for the Walnut Gulch and Little Washita watersheds is part of ongoing research.

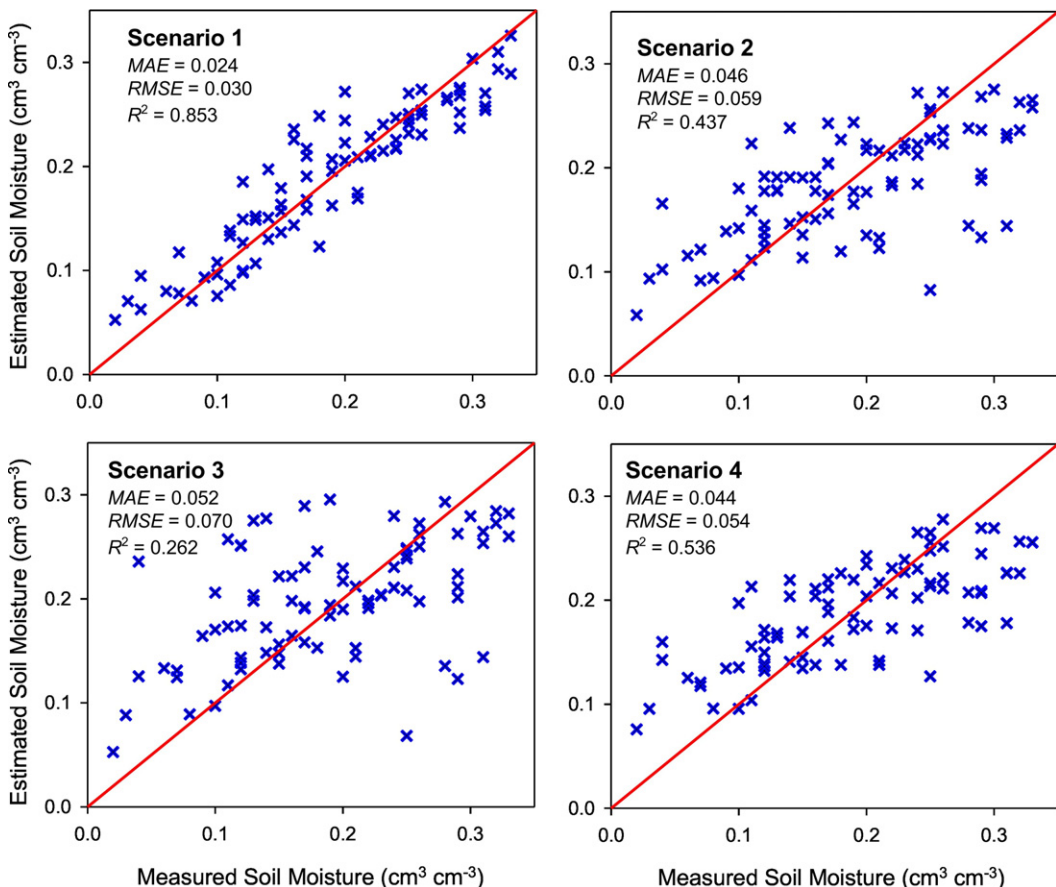


Fig. 11. Soil moisture estimates based on the Albedo-NDVI trapezoid model (parameterized based on the 4 different scenarios shown in Fig. 10) compared with in situ soil moisture measurements for the Little Washita watershed.

- (iii) Additional studies may improve the accuracy of OPTRAM through advancement of model formulation and parameterization, for example, by considering nonlinear dry and wet edges of the trapezoid similar to what has been done with TOTRAM (Mallick et al., 2009; Krapez et al., 2009). In order to exclude scattering due to unwanted oversaturated or shadowed pixels, the dry and wet edges were determined visually in scenario 1, which might introduce human bias. Improved masking of oversaturated or shadowed pixels or any other improvements leading to better defined edges could potentially advance OPTRAM through automation of this procedure.
- (iv) One basic assumption underlying OPTRAM is the linear relationship between root zone soil water content (θ) and vegetation water content (ω). In the derivation of Eq. (6) for vegetated soils (Appendix A), some previous studies reporting a close relation between ω and θ are cited. However, no experimental evidence for this relationship was found in the literature. Future laboratory, greenhouse and field research is required to explore to what extent and under what conditions this assumption is valid.
- (v) Previous studies (e.g., Ceccato et al., 2001, 2002) indicated that SWIR reflectance is not only sensitive to the leaf water content, but also to the leaf internal structure. Hence, combining the SWIR signal with an NIR band (primarily sensitive to the leaf internal structure) has been suggested to minimize the uncertainty in retrieving vegetation water content (Ceccato et al., 2002). This idea may be followed to reduce the site-dependency of OPTRAM parameters.

Acknowledgments

The authors gratefully acknowledge funding from National Science Foundation (NSF) grant no. 1521469. Additional support was provided by the Utah Agricultural Experiment Station, Utah State University, Logan, Utah 84322-4810, approved as UAES journal paper no. 8950.

Appendix A. Proof of Eq. (6) for vegetated soil

Based on the Kubelka and Munk (1931) two-flux radiative transfer model, Sadeghi et al. (2015) mathematically demonstrated that the relationship between SWIR reflectance of bare soil and its surface water content can be approximated with a linear relationship. Several studies indicated that the SWIR reflectance is sensitive to vegetation water content as well (Ceccato et al., 2001; Chen et al., 2005; Yilmaz et al., 2008). Here we demonstrate that the Sadeghi et al. (2015) analysis is also applicable for vegetated soils, yielding the same linear relationship between SWIR transformed reflectance, STR , and vegetation water content.

Let us first consider a fully vegetated soil, where soil vegetation cover is assumed to act as an absorbing/scattering layer with variable volumetric water content of ω [$L^3 L^{-3}$]. Assuming that the background soil does not contribute to the reflectance, reflectance of the vegetation layer, R , can be approximated with the Kubelka and Munk model:

$$R = 1 + \frac{K}{S} - \sqrt{\left(\frac{K}{S}\right)^2 + 2\frac{K}{S}} \quad (A1)$$

where $K [L^{-1}]$ and $S [L^{-1}]$ are the light absorption and scattering coefficients of the layer, respectively.

Inversion of Eq. (A1) yields:

$$r = \frac{K}{S} = \frac{(1-R)^2}{2R} \quad (A2)$$

where r is the transformed reflectance.

Treating the absorption and scattering coefficients of the vegetation layer as a simple additive function of absorption and scattering coefficients of its constituents, K and S of the layer can be formulated as (Sadeghi et al., 2015):

$$K = K_0 + K_{water}\omega \quad (A3)$$

$$S = S_0 + S_{water}\omega \quad (A4)$$

where subscripts “0” and “water” denote the fully dry vegetation layer and vegetation water, respectively.

Combining Eqs. (A2), (A3), and (A4) yields:

$$r = \frac{K_0 + K_{water}\omega}{S_0 + S_{water}\omega} \quad (A5)$$

Based on Eqs. (A3) and (A4), absorption and scattering coefficients of the vegetation layer at saturation ($\omega = \omega_s$) denoted as K_s and S_s can be defined as:

$$K_s = K_0 + K_{water}\omega_s \quad (A6)$$

$$S_s = S_0 + S_{water}\omega_s \quad (A7)$$

Combining Eqs. (A5), (A6), and (A7) yields the following r - ω relationship incorporating optical properties of fully dry and saturated vegetation layers:

$$r = \frac{K_0 \left(1 - \frac{\omega}{\omega_s}\right) + K_s \left(\frac{\omega}{\omega_s}\right)}{S_0 \left(1 - \frac{\omega}{\omega_s}\right) + S_s \left(\frac{\omega}{\omega_s}\right)} \quad (A8)$$

Eq. (A8) can be rearranged as follows:

$$r = \frac{\sigma r_0 \left(1 - \frac{\omega}{\omega_s}\right) + r_s \left(\frac{\omega}{\omega_s}\right)}{\sigma \left(1 - \frac{\omega}{\omega_s}\right) + \left(\frac{\omega}{\omega_s}\right)} \quad (A9)$$

where:

$$r_0 = \frac{K_0}{S_0} = \frac{(1-R_0)^2}{2R_0} \quad (A10)$$

$$r_s = \frac{K_s}{S_s} = \frac{(1-R_s)^2}{2R_s} \quad (A11)$$

$$\sigma = \frac{S_0}{S_s} = \frac{S_0}{S_0 + S_{water}\omega_s} \quad (A12)$$

where R_0 and R_s are the reflectance of a fully dry and saturated vegetation layer, respectively.

Eq. (A9) provides a nonlinear physically-based model for the r - ω relationship for the whole optical domain and is similar to Eq. (13) of Sadeghi et al. (2015) expressing the r - θ relationship in bare soils. At strong water absorbing wavelengths such as SWIR, the scattering coefficient of water is negligible (i.e., $S_{water} \approx 0$, $\sigma \approx 1$), and hence, Eq. (A9) reduces to a linear relationship:

$$\frac{\omega}{\omega_s} = \frac{STR - STR_0}{STR_s - STR_0} \quad (A13)$$

Writing Eq. (A13) once for a dry vegetation layer ($\omega = \omega_d$) corresponding to soil water content of θ_d and once for a wet vegetation layer ($\omega = \omega_w$) corresponding to soil water content of θ_w and

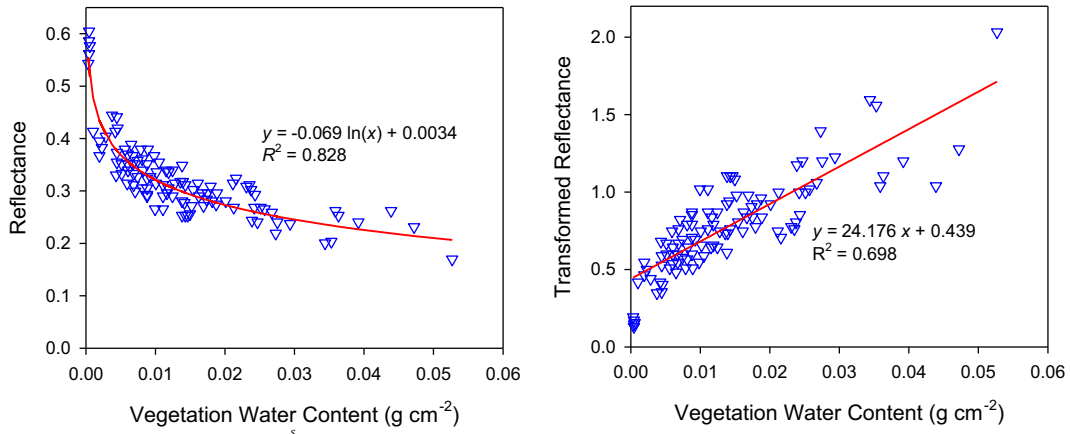


Fig. A1. Measured data showing correlation between reflectance (left, nonlinear) and transformed reflectance (right, nearly linear) at 1600 nm with vegetation water content [extracted from Fig. 3 of Ceccato et al. (2001)]. The measurements were performed with a laboratory spectroradiometer for various species of trees, crops and plants and primarily support the validity of Eq. (A13). Note that ω in Eq. (A13) is normalized with ω_s , and hence, the vegetation water content can be expressed in any arbitrary unit.

combining the two equations, we obtain:

$$\frac{\omega - \omega_d}{\omega_w - \omega_d} = \frac{STR - STR_d}{STR_w - STR_d} \quad (\text{A14})$$

Validity of the linear ω -STR relationship was primarily tested with measured data of Ceccato et al. (2001) for various species of trees, crops and plants (Fig. A1). Eq. (A14) would result in Eq. (6) for a fully vegetated soil, assuming that a linear relationship also holds between θ and ω (Note that θ is the root zone soil water content in this case). This assumption is based on previous studies reporting close relationships between leaf water deficit and soil moisture conditions (Rutter and Sands, 1958) and the fact that any soil moisture deficit can immediately affect plant water potential, which in turn affects cell turgor and relative water content of the living plant cells (Porporato et al., 2001).

It can be similarly shown that Eq. (6) holds true for any given fractional vegetation cover (i.e., partially vegetated soil), assuming that θ - ω relationship is linear. Assuming a partially vegetated surface with fixed fractional vegetation cover, FVC, the coefficients K and S of the surface layer can be formulated as:

$$K = K_0 + K_{water}\theta(1-FVC) + K_{water}\omega FVC \quad (\text{A15})$$

$$S = S_0 + S_{water}\theta(1-FVC) + S_{water}\omega FVC \quad (\text{A16})$$

where K_0 and S_0 are the absorption and scattering coefficients of the fully dry surface layer. Combining Eqs. (A5), (A15) and (A16) results in:

$$r = \frac{K_0 + K_{water}\theta(1-FVC) + K_{water}\omega FVC}{S_0 + S_{water}\theta(1-FVC) + S_{water}\omega FVC} \quad (\text{A17})$$

At SWIR wavelengths (i.e., $S_{water} \approx 0$), Eq. (A17) reduces to:

$$r = r_0 + \frac{K_{water}(1-FVC)}{S_0}\theta + \frac{K_{water}FVC}{S_0}\omega \quad (\text{A18})$$

Eq. (A18), in conjunction with the assumption of linearity of the θ - ω relationship, yields a linear r - θ relationship. Writing the resultant linear relationship once for a dry soil water content, θ_d , and once for a wet soil water content, θ_w , and combining the two equations, Eq. (6) is obtained.

References

- Amani, M., Parsian, S., MirMazloumi, S.M., Aieneh, O., 2016. Two new soil moisture indices based on the NIR-red triangle space of Landsat-8 data. *Int. J. Appl. Earth Obs. Geoinf.* 50, 176–186.
- Aminzadeh, M., Or, D., 2013. Temperature dynamics during nonisothermal evaporation from drying porous surfaces. *Water Resour. Res.* 49 (11), 7339–7349.
- Babaeian, E., Homaei, M., Montzka, C., Vereecken, H., Norouzi, A.A., van Genuchten, M.T., 2016. Soil moisture prediction of bare soil profiles using diffuse spectral reflectance information and vadose zone flow modeling. *Remote Sens. Environ.* 187, 218–229.
- Carlson, T.N., 2007. An overview of the "triangle method" for estimating surface evapotranspiration and soil moisture from satellite imagery. *Sensors* 7 (8), 1612–1629.
- Carlson, T.N., 2013. Triangle models and misconceptions. *Int. J. Remote. Sens. Appl.* 3 (3), 155–158.
- Carlson, T.N., Gillies, R.R., Perry, E.M., 1994. A method to make use of thermal infrared temperature and NDVI measurements to infer surface soil water content and fractional vegetation cover. *Remote Sens. Rev.* 9 (1–2), 161–173.
- Ceccato, P., Flasse, S., Tarantola, S., Jacquemoud, S., Grégoire, J.M., 2001. Detecting vegetation leaf water content using reflectance in the optical domain. *Remote Sens. Environ.* 77 (1), 22–33.
- Ceccato, P., Gobron, N., Flasse, S., Pinty, B., Tarantola, S., 2002. Designing a spectral index to estimate vegetation water content from remote sensing data: part 1: theoretical approach. *Remote Sens. Environ.* 82 (2), 188–197.
- Chen, D., Huang, J., Jackson, T.J., 2005. Vegetation water content estimation for corn and soybeans using spectral indices derived from MODIS near-and short-wave infrared bands. *Remote Sens. Environ.* 98 (2), 225–236.
- Cosh, M.H., Jackson, T.J., Starks, P., Heathman, G., 2006. Temporal stability of surface soil moisture in the Little Washita River watershed and its applications in satellite soil moisture product validation. *J. Hydrol.* 323 (1), 168–177.
- Crow, W.T., Kustas, W.P., Prueger, J.H., 2008. Monitoring root-zone soil moisture through the assimilation of a thermal remote sensing-based soil moisture proxy into a water balance model. *Remote Sens. Environ.* 112 (4), 1268–1281.
- Das, N.N., Mohanty, B.P., Njoku, E.G., 2008, July. Characterization of backscatter by surface features in L-band active microwave remote sensing of soil moisture. *IGARSS 2008–2008 IEEE International Geoscience and Remote Sensing Symposium*. vol. 2. IEEE, pp. II-817.
- Entekhabi, D., Yueh, S., O'Neill, P.E., Kellogg, K.H., Allen, A., Bindlish, R., Brown, M., Chan, S., Collander, A., Crow, W.T., Das, N., 2014. *SMAP Handbook–Soil Moisture Active Passive: Mapping Soil Moisture and Freeze/Thaw from Space*.
- Feng, H., Chen, C., Dong, H., Wang, J., Meng, Q., 2013. Modified shortwave infrared perpendicular water stress index: a farmland water stress monitoring method. *J. Appl. Meteorol. Climatol.* 52 (9), 2024–2032.
- Fensholt, R., Sandholt, I., 2003. Derivation of a shortwave infrared water stress index from MODIS near- and shortwave infrared data in a semiarid environment. *Remote Sens. Environ.* 87 (1), 111–121.
- Feyisa, G.L., Meilby, H., Fensholt, R., Proud, S.R., 2014. Automated water extraction index: a new technique for surface water mapping using Landsat imagery. *Remote Sens. Environ.* 140, 23–35.
- Frazier, P.S., Page, K.J., 2000. Water body detection and delineation with Landsat TM data. *Photogramm. Eng. Remote. Sens.* 66 (12), 1461–1468.
- Ghulam, A., Qin, Q., Wang, L., Zhan, Z., Wang, D., 2004, September. Development of broadband Albedo based ecological safety monitoring index. *Geoscience and Remote Sensing Symposium, 2004. IGARSS'04. Proceedings. 2004 IEEE International*. vol. 6. IEEE, pp. 4115–4118.
- Ghulam, A., Qin, Q., Zhan, Z., 2007a. Designing of the perpendicular drought index. *Environ. Geol.* 52 (6), 1045–1052.
- Ghulam, A., Qin, Q., Teyip, T., Li, Z.L., 2007b. Modified perpendicular drought index (MPDI): a real-time drought monitoring method. *ISPRS J. Photogramm. Remote Sens.* 62 (2), 150–164.
- Ghulam, A., Li, Z.L., Qin, Q., Tong, Q., Wang, J., Kasimu, A., Zhu, L., 2007c. A method for canopy water content estimation for highly vegetated surfaces–shortwave infrared perpendicular water stress index. *Sci. China Ser. D Earth Sci.* 50 (9), 1359–1368.

- Ghulam, A., Li, Z.L., Qin, Q., Tong, Q., 2007d. Exploration of the spectral space based on vegetation index and albedo for surface drought estimation. *J. Appl. Remote. Sens.* 1 (1), 013529.
- Gillies, R.R., Kustas, W.P., Humes, K.S., 1997. A verification of the 'triangle' method for obtaining surface soil water content and energy fluxes from remote measurements of the Normalized Difference Vegetation Index (NDVI) and surface e. *Int. J. Remote Sens.* 18 (15), 3145–3166.
- Goward, S.N., Xue, Y., Czajkowski, K.P., 2002. Evaluating land surface moisture conditions from the remotely sensed temperature/vegetation index measurements: an exploration with the simplified simple biosphere model. *Remote Sens. Environ.* 79 (2), 225–242.
- Han, Y., Wang, Y., Zhao, Y., 2010. Estimating soil moisture conditions of the greater Changbai Mountains by land surface temperature and NDVI. *IEEE Trans. Geosci. Remote Sens.* 48 (6), 2509–2515.
- Hassan-Esfahani, L., Torres-Rua, A., Jensen, A., McKee, M., 2015. Assessment of surface soil moisture using high-resolution multi-spectral imagery and artificial neural networks. *Remote Sens.* 7 (3), 2627–2646.
- Jackson, T.J., Cosh, M.H., Goodrich, D., Moran, S., Keefer, T., 2009. SMEX04 Walnut Gulch Experimental Watershed Soil Moisture Data: Arizona. NASA DAAC at the National Snow and Ice Data Center, Boulder, Colorado USA.
- Jackson, T.J., Bindlish, R., Cosh, M.H., Zhao, T., Starks, P.J., Bosch, D.D., Seyfried, M., Moran, M.S., Goodrich, D.C., Kerr, Y.H., Leroux, D., 2012. Validation of Soil Moisture and Ocean Salinity (SMOS) soil moisture over watershed networks in the US. *IEEE Trans. Geosci. Remote Sens.* 50 (5), 1530–1543.
- Janatian, N., Sadeghi, M., Sanaeinejad, S.H., Bakhshian, E., Farid, A., Hasheminia, S.M., Ghazanfari, S., 2017. A statistical framework for estimating air temperature using MODIS land surface temperature data. *Int. J. Climatol.* 37, 1181–1194.
- Keefer, T.O., Moran, M.S., Paige, G.B., 2008. Long-term meteorological and soil hydrology database, Walnut Gulch Experimental Watershed, Arizona, United States. *Water Resour. Res.* 44 (5), W05007.
- Kingsford, R.T., Thomas, R.F., Wong, P.S., Knowles, E., 1997. GIS Database for Wetlands of the Murray Darling Basin, Final Report of the Murray Darling Basin Commission. National Parks and Wildlife Service, Sydney, Australia.
- Krapež, J.C., Olioso, A., Coudert, B., 2009, September. Comparison of three methods based on the Temperature-NDVI diagram for soil moisture characterization. In: Neale, C.M., Maltese, A. (Eds.), Proc. of SPIE Vol. vol. 7472, p. 74720Y-1.
- Kubelka, P., Munk, F., 1931. Ein Beitrag zur Optik der Farbanstriche. *Zeitschrift für Technische Physik* 12, 593–601.
- Liang, S., 2000. Narrowband to broadband conversions of land surface albedo I: algorithms. *Remote Sens. Environ.* 76 (2), 213–238.
- Liu, S., Roberts, D.A., Chadwick, O.A., Still, C.J., 2012. Spectral responses to plant available soil moisture in a California grassland. *Int. J. Appl. Earth Obs. Geoinf.* 19, 31–44.
- Mallick, K., Bhattacharya, B.K., Patel, N.K., 2009. Estimating volumetric surface moisture content for cropped soils using a soil wetness index based on surface temperature and NDVI. *Agric. For. Meteorol.* 149 (8), 1327–1342.
- Mladenova, I.E., Jackson, T.J., Njoku, E., Bindlish, R., Chan, S., Cosh, M.H., Holmes, T.R.H., De Jeu, R.A.M., Jones, L., Kimball, J., Paloscia, S., 2014. Remote monitoring of soil moisture using passive microwave-based techniques—theoretical basis and overview of selected algorithms for AMSR-E. *Remote Sens. Environ.* 144, 197–213.
- Moran, M.S., Clarke, T.R., Inoue, Y., Vidal, A., 1994. Estimating crop water deficit using the relation between surface-air temperature and spectral vegetation index. *Remote Sens. Environ.* 49 (3), 246–263.
- Nemani, R., Pierce, L., Running, S., Goward, S., 1993. Developing satellite-derived estimates of surface moisture status. *J. Appl. Meteorol.* 32 (3), 548–557.
- Nichols, S., Zhang, Y., Ahmad, A., 2011. Review and evaluation of remote sensing methods for soil-moisture estimation. *J. Photonics Energy* 2, 028001.
- Njoku, E.G., Entekhabi, D., 1996. Passive microwave remote sensing of soil moisture. *J. Hydrol.* 184 (1), 101–129.
- Ochsner, T.E., Cosh, M.H., Cuenco, R.H., Dorigo, W.A., Draper, C.S., Hagimoto, Y., Kerr, Y.H., Njoku, E.G., Small, E.E., Zreda, M., 2013. State of the art in large-scale soil moisture monitoring. *Soil Sci. Soc. Am. J.* 77 (6), 1888–1919.
- Patel, N.R., Anapashsha, R., Kumar, S., Saha, S.K., Dadhwal, V.K., 2009. Assessing potential of MODIS derived temperature/vegetation condition index (TVDI) to infer soil moisture status. *Int. J. Remote Sens.* 30 (1), 23–39.
- Peng, C., Deng, M., Di, L., 2014. Relationships between remote-sensing-based agricultural drought indicators and root zone soil moisture: a comparative study of Iowa. *IEEE J. Sel. Top. Appl. Earth Observ. Remote. Sens.* 7 (11), 4572–4580.
- Petroppoulos, G., Carlson, T.N., Wooster, M.J., Islam, S., 2009. A review of Ts/VI remote sensing based methods for the retrieval of land surface energy fluxes and soil surface moisture. *Prog. Phys. Geogr.* 33 (2), 224–250.
- Porporato, A., Laio, F., Ridolfi, L., Rodriguez-Iturbe, I., 2001. Plants in water-controlled ecosystems: active role in hydrologic processes and response to water stress: III. Vegetation water stress. *Adv. Water Resour.* 24 (7), 725–744.
- Pratt, D.A., Ellyett, C.D., 1979. The thermal inertia approach to mapping of soil moisture and geology. *Remote Sens. Environ.* 8 (2), 151–168.
- QGIS Development Team, 2016. QGIS Geographic Information System. Open Source Geospatial Foundation Project. <http://www.qgis.org/>.
- Qin, Z., Karnieli, A., Berliner, P., 2001. A mono-window algorithm for retrieving land surface temperature from Landsat TM data and its application to the Israel-Egypt border region. *Int. J. Remote Sens.* 22 (18), 3719–3746.
- Qin, Q., Jin, C., Zhang, N., Yang, X., 2010, July. An two-dimensional spectral space based model for drought monitoring and its re-examination. *Geoscience and Remote Sensing Symposium (IGARSS), 2010 IEEE International.* IEEE, pp. 3869–3872.
- Rahimzadeh-Bajgiran, P., Berg, A.A., Champagne, C., Omasa, K., 2013. Estimation of soil moisture using optical/thermal infrared remote sensing in the Canadian Prairies. *ISPRS J. Photogramm. Remote Sens.* 83, 94–103.
- Renard, K.G., Lane, L.J., Simanton, J.R., Emmerich, W.E., Stone, J.J., Weltz, M.A., Goodrich, D.C., Yakowitz, D.S., 1993. Agricultural impacts in an arid environment: Walnut Gulch studies. *Hydrolog. Sci. Technol.* 9 (1–4), 145–190.
- Robinson, D.A., Campbell, C.S., Hopmans, J.W., Hornbuckle, B.K., Jones, S.B., Knight, R., Ogden, F., Selker, J., Wendroth, O., 2008. Soil moisture measurement for ecological and hydrological watershed-scale observatories: a review. *Vadose Zone J.* 7 (1), 358–389.
- Rutter, A.J., Sands, K., 1958. The relation of leaf water deficit to soil moisture tension in *Pinus sylvestris* L. *New Phytol.* 57 (1), 50–65.
- Sadeghi, M., Jones, S.B., Philpot, W.D., 2015. A linear physically-based model for remote sensing of soil moisture using short wave infrared bands. *Remote Sens. Environ.* 164, 66–76.
- Sadeghi, M., Tabatabaeenejad, A., Tuller, M., Moghaddam, M., Jones, S.B., 2017. Advancing the AirMOSS P-band radar root zone soil moisture retrieval algorithm via incorporation of Richards' equation. *Remote Sens.* 9 (1):1–17. <http://dx.doi.org/10.3390/rs9010017>.
- Sandholt, I., Rasmussen, K., Andersen, J., 2002. A simple interpretation of the surface temperature/vegetation index space for assessment of surface moisture status. *Remote Sens. Environ.* 79 (2), 213–224.
- Santos, W.J.R., Silva, B.M., Oliveira, G.C., Volpato, M.M.L., Lima, J.M., Curi, N., Marques, J.J., 2014. Soil moisture in the root zone and its relation to plant vigor assessed by remote sensing at management scale. *Geoderma* 221, 91–95.
- Schnur, M.T., Xie, H., Wang, X., 2010. Estimating root zone soil moisture at distant sites using MODIS NDVI and EVI in a semi-arid region of southwestern USA. *Eco. Inform.* 5 (5), 400–409.
- Shafan, S., 2014. Estimation of Soil Moisture Status in the Texas High Plains Using Remote Sensing. Doctoral dissertation. Texas Tech University.
- Shafan, S., Maas, S.J., 2015a. Index of soil moisture using raw Landsat image digital count data in Texas high plains. *Remote Sens.* 7 (3), 2352–2372.
- Shafan, S., Maas, S.J., 2015b. Improvement of the Trapezoid method using raw Landsat image digital count data for soil moisture estimation in the Texas (USA) High Plains. *Sensors* 15 (1), 1925–1944.
- Starks, P.J., Fiebrich, C.A., Grimsley, D.L., Garbrecht, J.D., Steiner, J.L., Guzman, J.A., Moriasi, D.N., 2014. Upper Washita River experimental watersheds: meteorologic and soil climate measurement networks. *J. Environ. Qual.* 43 (4), 1239–1249.
- Stisen, S., Sandholt, I., Nørgaard, A., Fenesholt, R., Jensen, K.H., 2008. Combining the triangle method with thermal inertia to estimate regional evapotranspiration: applied to MSG-SEVIRI data in the Senegal River basin. *Remote Sens. Environ.* 112 (3), 1242–1255.
- Stratoulas, D., Balzter, H., Sykoti, O., Zlinszky, A., Tóth, V.R., 2015. Evaluating sentinel-2 for lakeshore habitat mapping based on airborne hyperspectral data. *Sensors* 15 (9), 22956–22969.
- Sun, H., 2016. Two-stage trapezoid: a new interpretation of the land surface temperature and fractional vegetation coverage space. *IEEE J. Sel. Top. Appl. Earth Observ. Remote. Sens.* 9 (1), 336–346.
- Tabatabaeenejad, A., Burgin, M., Duan, X., Moghaddam, M., 2015. P-band radar retrieval of subsurface soil moisture profile as a second-order polynomial: first AirMOSS results. *IEEE Trans. Geosci. Remote Sens.* 53 (2), 645–658.
- Tian, J., Philpot, W.D., 2015. Relationship between surface soil water content, evaporation rate, and water absorption band depths in SWIR reflectance spectra. *Remote Sens.* Environ.
- United States Geological Survey, 2016. Landsat 8 Operational Land Imager and Thermal Infrared Sensor Calibration Notices.
- Van de Griend, A.A., Owe, M., 1993. On the relationship between thermal emissivity and the normalized difference vegetation index for natural surfaces. *Int. J. Remote Sens.* 14 (6), 1119–1131.
- Vereecken, H., Huisman, J.A., Bogaena, H., Vanderborght, J., Vrugt, J.A., Hopmans, J.W., 2008. On the value of soil moisture measurements in vadose zone hydrology: a review. *Water Resour. Res.* 44 (4), WOOD006.
- Verstraeten, W.W., Veroustraete, F., van der Sande, C.J., Grootaers, I., Feyen, J., 2006. Soil moisture retrieval using thermal inertia, determined with visible and thermal spaceborne data, validated for European forests. *Remote Sens. Environ.* 101 (3), 299–314.
- Wan, Z., Wang, P., Li, X., 2004. Using MODIS land surface temperature and normalized difference vegetation index products for monitoring drought in the southern Great Plains, USA. *Int. J. Remote Sens.* 25 (1), 61–72.
- Wang, L., Qu, J.J., 2009. Satellite remote sensing applications for surface soil moisture monitoring: a review. *Front. Earth Sci. China* 3 (2), 237–247.
- Wang, X., Xie, H., Guan, H., Zhou, X., 2007. Different responses of MODIS-derived NDVI to root-zone soil moisture in semi-arid and humid regions. *J. Hydrol.* 340 (1), 12–24.
- Wang, W., Huang, D., Wang, X.G., Liu, Y.R., Zhou, F., 2011. Estimation of soil moisture using trapezoidal relationship between remotely sensed land surface temperature and vegetation index. *Hydrol. Earth Syst. Sci.* 15 (5), 1699–1712.
- Wang, F., Qin, Z., Song, C., Tu, L., Karnieli, A., Zhao, S., 2015. An improved mono-window algorithm for land surface temperature retrieval from Landsat 8 thermal infrared sensor data. *Remote Sens.* 7 (4), 4268–4289.
- Whiting, M.L., Li, L., Ustin, S.L., 2004. Predicting water content using Gaussian model on soil spectra. *Remote Sens. Environ.* 89 (4), 535–552.
- Xie, H., Luo, X., Xu, X., Pan, H., Tong, X., 2016. Evaluation of Landsat 8 OLI imagery for unsupervised inland water extraction. *Int. J. Remote Sens.* 37 (8), 1826–1844.
- Yilmaz, M.T., Hunt, E.R., Jackson, T.J., 2008. Remote sensing of vegetation water content from equivalent water thickness using satellite imagery. *Remote Sens. Environ.* 112 (5), 2514–2522.

- Zeng, W., Xu, C., Huang, J., Wu, J., Tuller, M., 2016. Predicting near-surface soil moisture content of saline soils from NIR reflectance spectra with a Modified Gaussian model. *Soil Sci. Soc. Am. J.* <http://dx.doi.org/10.2136/sssaj2016.06.0188>.
- Zhang, D., Zhou, G., 2016. Estimation of soil moisture from optical and thermal remote sensing: a review. *Sensors* 16 (8), 1308.
- Zhang, J., Wang, Y., Li, Y., 2006. A C++ program for retrieving land surface temperature from the data of Landsat TM/ETM + band6. *Comput. Geosci.* 32 (10), 1796–1805.
- Zhang, N., Hong, Y., Qin, Q., Liu, L., 2013. VSDI: a visible and shortwave infrared drought index for monitoring soil and vegetation moisture based on optical remote sensing. *Int. J. Remote Sens.* 34 (13), 4585–4609.
- Zhang, D., Tang, R., Zhao, W., Tang, B., Wu, H., Shao, K., Li, Z.L., 2014. Surface soil water content estimation from thermal remote sensing based on the temporal variation of land surface temperature. *Remote Sens.* 6 (4), 3170–3187.